ASN NEURO Immediate Publication. Published on 7 August 2009 as manuscript AN20090028

TITLE: Different Proteolipid Protein Mutants Exhibit Unique Metabolic Defects

AUTHORS: [2]Maik Hüttemann, [1]Zhan Zhang, [1]Chadwick Mullins, [1]Denise Bessert, [2]Icksoo Lee, [3]Klaus-Armin Nave, [1]Sunita Appikatla and [1,2]Robert P. Skoff

AUTHOR AFFILIATIONS: [1]Department of Anatomy and Cell Biology, [2]Center for Molecular Medicine and Genetics, [1,2]Wayne State University School of Medicine, Detroit MI and [3]Department of Neurogenetics, Max Planck Institute of Experimental Medicine, Göttingen, Germany

ABBREVIATED TITLE: Mitochondrial Defects in *Plp1* Mutants

CORRESPONDING AUTHOR: Robert P. Skoff Dept. of Anatomy and Cell Biology Wayne State University School of Medicine 540 E. Canfield Detroit MI 48201 rskoff@med.wayne.edu, ph 313.577.1165; FAX 313.577.3377

KEYWORDS: mitochondria, oligodendrocytes, oxidative phosphorylation, Pelizaeus-Merzbacher Disease, Plp1 mutants

LIST OF ABBREVIATIONS: AIF, apoptosis inducing factor; CcO, cytochrome c oxidase; $\Delta\psi_m$, mitochondrial membrane potential; ER, endoplasmic reticulum; EM, electron microscopy; IMM, inner mitochondrial membrane; jp, jimpy mouse; mtCK, mitochondrial creatine kinase; Olg, oligodendrocyte; OMM, outer mitochondrial membrane; PARP, poly (ADP-ribose) polymerase; *Plp1*, X-linked myelin proteolipid protein gene; *Plp1*tg, mice with Plp1 duplications; PMD, Pelizaus-Merzbacher Disease; UPR, unfolded protein response

ABSTRACT

Pelizaeus-Merzbacher Disease (PMD), a CNS disease characterized by shortened life span and severe neural dysfunction, is caused by mutations of the X-linked myelin proteolipid protein (*PLP1*) gene. The majority of human *PLP1* mutations are caused by duplications; almost all others are caused by missense mutations. The cellular events leading to the phenotype are unknown. The same mutations in non-humans make them ideal models to study the mechanisms that cause neurological sequelae. We show that mice with *Plp1* duplications (*Plp1*tg) have major mitochondrial deficits with a 50% reduction of ATP, a drastically reduced mitochondrial membrane potential, and increased numbers of mitochondria. In contrast, the jimpy (jp) mouse with a *Plp1* missense mutation exhibits normal mitochondrial function. We show that PLP in the *Plp1tg* mice and in *Plp1* transfected cells is targeted to mitochondria. PLP has motifs permissive for insertion into mitochondria; deletions near its N-terminus prevent its co-localization to mitochondria. This novel data shows that *Plp1* missense mutations and duplications of native *Plp1* gene initiate uniquely different cellular responses.

INTRODUCTION

Pelizaeus-Merzbacher Disease is caused by mutations in the CNS X-linked proteolipid protein 1 (*PLP1*) gene (Hodes et al., 1993; Boespflug-Tanguy, 1994; Ellis and Malcolm, 1994). *PLP1* mutations fall into 4 broad classes: (1) duplications of the native (wild-type) gene, (2) point mutations, (3) deletions, and (4) frame shift mutations. Duplications account for nearly 70% of human *PLP1* mutations (Garbern et al., 1999; Garbern, 2007). In many men, the duplications are lethal, with death ensuing within the first decade. No treatments are available for PMD patients except for medications to counteract seizures and spasticity. The sequence of cellular events that cause neurological dysfunction and ultimately death is poorly understood in PMD patients. Because *Plp1* mutations in animals are often identical to those in humans and both present with similar motor deficits, they are useful models to study PMD.

An unfolded protein response (UPR) has been demonstrated in rodents and in cell lines with missense mutations (Southwood et al., 2002; McLaughlin et al., 2007) and in cell lines that over-express mutant *Plp1* (Dhaunchak and Nave, 2007). Not surprisingly, trafficking of mutant PLP to the plasma membrane is altered (Thomson et al., 1997). In animals with missense mutations, this UPR and aberrant protein trafficking is thought to cause oligodendrocyte (Olg) malfunction. However, in rodents with duplications of the *Plp1* gene, investigation of cellular and molecular events is limited. In mice with low *Plp1* gene copy number, abnormal accumulation of PLP in the endoplasmic reticulum (ER) and a subsequent UPR is barely detectable (Cerghet et al., 2001). Moreover, it is apparently lacking in Olgs transfected with wild-type PLP (Kramer-Albers et al., 2006). We also observed major differences in expression of apoptotic markers between these two mutants. (For example, we surprisingly found that apoptosis inducing factor (AIF) was translocated into nuclei of *Plp1*tg mice 4x greater than in jp (Supplemental Figure 1). We predicted the reverse results because apoptosis is about 3-4 fold less in *Plp1*tgs than in jp (Cerghet et al., 2001). Translocation of AIF to nuclei is significant in understanding cell death pathways because this protein is highly up-regulated in the caspase-independent or mitochondrially-dependent pathway (Cregan et al., 2004; Haeberlein, 2004). Moreover, it is activated in response to poly(ADP-ribose) polymerase (PARP) activation which we also found elevated in the *Plp1*tg mice (Cerghet et al., 2001). These observations, taken together, suggest that different cell death pathways operate in the two major classes of *Plp1* mutations. Here, we examine mitochondrial function in the two mutants and show for the first time that mice with duplications of *Plp1* gene exhibit major mitochondrial defects.

MATERIALS AND METHODS

Animals, Phenotyping, and Genotyping. All animals were housed in the Division of Laboratory Animal Resources, a federally approved animal facility, and all procedures were approved by the Wayne State University Animal Investigation Committee. Plp1/^{jp} jimpy /Tabby female carriers (jp+/+Ta) and males (+Ta) were purchased from Jackson Laboratories (Bar Harbor, ME). Jp mice were genotyped by PCR. Tails were cut from neonatal mice, DNA isolated and purified with Extract-N-Amp Tissue PCR Kit (Sigma, St. Louis, MO), and PCR performed using primers 5'-CATGCCTCTAGCCTTATGAAGTTAC-3' and 5'-CTTCAGCTGTTTTGCAGATGGACAG-3' that amplifies a portion of intron 4 and exon 5 which includes a Dde I site. The DNA is digested with Dde1, resolved on a 6% acrylamide gel, and visualized with ethidium bromide. The Dde I restriction site is lost in jp so amplified DNA, when digested with Dde I, will yield 1 band at 125bp for jp males, 2 bands at 75 and 50bp for wild-type males and females and all three bands for heterozygous females.

*Plp1*tg line 66 mice were obtained from C. Readhead (Cedars-Sinai Hospital, Los Angeles, CA). The seven exon transcription *Plp1* mouse unit and 3.5kb of the *Plp1* 5' regulatory unit were used to generate line 66 transgenic mice (Readhead et al., 1994). Most *Plp1*tg mice develop tremors between 25-40 days after birth followed by seizures a few days later. All mice used in this study exhibited tremors and/or seizures. In our initial studies, offspring from *Plp1*tg carrier mice were identified following the procedure of Readhead et al., (1994) for the presence or absence of the T7 promoter sequence contained in the inserted vector. Tails were cut from neonatal mice, DNA isolated and purified as described above, PCR performed using primers 5'-CAGGTGTTGAGTCTGATCTACACAAG-3' and 5'-GCATAATACGACTCACTATAGGGATC-3'. PCR products were resolved on a 1.5% agarose gel, and visualized with ethidium bromide. Transgenic mice have a 250 bp product. In later studies, *Plp1*tg mice were genotyped using real-time PCR (Regis et al., 2005). DNA was isolated from neonatal mice tails and purified with DNeasy Tissue Kit (QIAGEN, Valencia, CA). The oligonucleotide primers specific for exon 3 of the *Plp1* gene (5'- GGGCTCCAGAACATCATCC-3' and 3'-GTCCACCACTGACACGTTGG-5') were used to amplify a 131 bp product. The *Plp1* gene dosage was determined by relative quantitative comparative threshold cycle method ($\Delta\ \Delta$Ct). Primers specific for exon 7 of the GAPDH gene served as an endogenous reference gene. Amplification of GAPDH and Plp1 were run simultaneously in separate tubes. Males with more than 2 extra copies and females with more than 4 extra copies usually exhibited behavioural abnormalities.

ATP measurements. All mice were starved for 5-6 hrs beginning in the morning; H_20 was provided *ad libitum*. Mice were sacrificed by cervical dislocation, brains immediately excised, frozen in liquid N_2 and stored at -80°C until measurement. In order to release cellular ATP, frozen tissue (25 mg) was boiled for 2 min after the addition of 300 μL of H_2O containing 100 mM Tris-HCl (pH 7.75) and 4 mM EDTA. Samples were put on ice and homogenized by sonification (micro tip, 1x10 sec pulse). ATP concentrations were determined in triplicates per animal with the ATP bioluminescence assay kit HS II

(Roche Basal, Switzerland) according to the manufacturer's protocol using an Optocomp 1 luminometer (MGM Instruments, Hamden CT). Data were standardized to the protein concentration which was determined using the DC protein assay kit (Bio-Rad, Hercules CA). Data were expressed as the mean ± standard error of the mean (SEM) over 3 independent measurements per animal. Significance between multiple groups was determined using one-way analysis of variance (ANOVA).

CcO brain measurements. CcO activity was determined as previously described (Lee et al; 2005) with modifications. Brain plugs (25 mg) were solubilized in 500 µl chilled measuring buffer (10 mM K-HEPES (pH 7.4), 40 mM KCl, 1% Tween 20, 2 µM oligomycin, 1 mM PMSF, 10 mM KF, 1 mM Na-vanadate, 2 mM EGTA) using a Teflon microtube pestle applying 5 strokes followed by sonification (micro tip, 3x10 sec pulses). Cell debris was removed by centrifugation (2 min, 16,000x g) and the supernatant used for respiration measurements. Protein concentration was determined using the DC protein assay kit (Bio-Rad). CcO activity was determined at 25°C in a closed 200 µL chamber containing a micro Clark-type oxygen electrode (Oxygraph system, Hansatech Instruments, Pentney, King's Lynn, Norfolk, England) by increasing the amount of substrate cytochrome *c*. Since CcO is regulated by adenine nucleotides (Napiwotzki et al., 1997), measurements were performed in the presence of 5 mM ADP or 5 mM ATP including an ATP regenerating system (Lee et al., 2002). Oxygen consumption was recorded on a computer and calculated using the Oxygraph software (Hansatech). Turnover number (TN) is defined as consumed O_2 ((µM)/(min·total protein (mg)).

CcO histochemistry.
CcO activity was measured on 15 µm frozen brain sections at the level of the striatum (Wong-Riley, 1979) with modifications (Hüttemann M, et al., 2007). Briefly, slides were transferred from -80°C to room temperature and tissue sections were circled with a hydrophobic pen, allowing the application of small reaction buffer volumes. 100 µL of freshly prepared reaction buffer (100 mM KH_2PO_4, pH 7.4, 4% sucrose, 0.50 mg/mL diaminobenzidine (DAB), 200 µg/mL catalase, 0.15 µg/mL cow heart cytochrome *c*) was added to each section, and slides were incubated in a moist chamber for 20 min at 37°C in the dark. The reaction was terminated by washing the slides 3x in 100 mM KH_2PO_4 (pH 7.4). Slides were rinsed once in dH_2O and air dried for 3 hr and mounted with Permount. For semi-quantitative assessment of the intensity of the CcO histochemical reaction, images were captured with a SPOT Flex Camera (Diagnostic Instruments Inc.) attached to a Leitz Laborlux 12 Microscope equipped with a 25X objective. The white balance was adjusted for the slide before taking images so the same background was used for both *Plp1tg* and control. Images taken from the dorsal medial striatum, ventral lateral striatum, corpus callosum, hippocampus, and cortex of both *Plp1tg* and control sections, both of which were on the same slide, were taken at 24 bits per pixel RGB. Images were opened in Adobe Photoshop, inverted and 3 histograms including an area of 300 x 300 pixels were obtained, averaged and compared between *Plp1*tg and controls. Brains from 6 *Plp1tg* and 6 controls were analyzed. Statistical analysis (ANOVA) was used to determine differences between groups. The average of *Plp1*tg was reported as the percent increase over the average histogram of control sections.

Mitochondrial membrane potential ($\Delta\Psi_m$). We first measured $\Delta\Psi_m$ with the probe JC-1 (Invitrogen, Carlsbad, CA) in transfected COS7 cells and secondly ex vivo in brain slices. Cells grown on 12mm coverslips, were transiently transfected using Lipofectamine (Invitrogen) with a N-terminal EGFP linked full-length PLP cDNA when cells were approximately 70% confluent (see below). Cell were also transfected with P0-EGFP, Na^+ channel β-subunit-EGFP, PMP-22-EGFP and LacZ-EGFP. Eight or twenty-four hrs after transfection, JC-1 was added to the cells (10 μg/ml) in cell growth media. Cells were incubated at 37ºC, 5% CO_2 for 15 minutes. Media was replaced with fresh media, cells incubated for 15 minutes, washed 3 times in PBS, mounted in PBS and immediately imaged. Images were obtained on a Leica DMIRB Microscope equipped with a 20X objective using a SPOT RT Slider camera and images were compiled in Adobe Photoshop. The green monomeric form of JC-1 is excited at 485 nm and emits at 535 nm; the red aggregate form is excited at 550 nm, and emits at 600 nm. Red and green can be imaged either simultaneously or individually using the appropriate filters. However, excitation with a FITC filter for green JC-1, also excites EGFP making the two difficult to distinguish.

For in vivo measurements, unfixed brains were immediately removed, 100μm sections were cut on a Vibratome in PBS at 37°C, collected in PBS 37°C, first incubated in DMEM for 5 min at 37°C with 5% CO_2, next in DMEM containing 3.33μg/ml JC-1 for 30 min, and last in DMEM w/o JC-1 for 20 min, rinsed twice in PBS and mounted on glass slides with a coverslip in PBS. Slices were photographed within several minutes after rinsing. Images were captured as above.

Cellular fractionation and Western blotting. Mitochondrial/cytosolic and nuclear/cytosolic fractionation kits were used following the manufacturers instructions (Biovision, Mountain View, CA). To confirm the purity of the mitochondrial fractions, Westerns were probed with markers for Golgi (Golgin 97, Molecular Probes, Eugene OR), Endoplasmic reticulum (anti-KDEL, StressGen, Victoria BC, Canada), lysosomes (anti-LAMP2, ABR, Golden CO), mitochondria (anti-CcO, Molecular Probes, OR) crude plasma membrane fractions (anti-NG2, Chemicon, Billerica MA), pan-sodium channel and β-actin (Sigma) and a PLP antibody directed against the PLP specific domain generated for the Skoff lab by ABR (Rockford IL). Blots were lightly stripped and reprobed as many as 6 times. For antigens with higher molecular weights (above 180kD), the same homogenates were used but run on an 8% gel rather than our standard 4-12% gel. 100μg fractions were loaded into each lane except for brain homogenates when 20 μg were loaded. Each gel was transferred onto a PVDF membrane, membranes blocked with 8% milk, incubated in antibody overnight, washed, incubated with secondary antibody, washed and detected using ChemiLucent Detection System (Chemicon, Billerica, MA). In a separate experiment, cytosolic and mitochondrial fractions were probed for MBP (Sternberger Monoclonals, Baltimore, MD) and PLP/DM20 against the C-terminus generated for the Skoff lab by ABR. 100μg of cytosolic and mitochondrial fractions along with 25μg of whole brain homogenate were run on a 4-12% gel and transferred to PVDF membrane. Membranes were processed as described above and MBP detected using the ChemiLucent Detection System (Chemicon), stripped and reprobed for C-terminal PLP and DM20, and again for β-actin.

PLP Plasmid Construction. Plasmid clone 68 of pDM100 (pDM100.68) contained a full-length cDNA for mouse *Plp1* (kindly provided by AT Campagnoni, UCLA, Los Angeles CA). Full-length cDNA of mouse *Plp1* was amplified by PCR and cloned into the pEGFP-N1 and pAcGFP-C1 vectors (Clontech, USA) at the EcoRI/BamHI site to produce two different constructs. The constructs are N-terminal PLP-EGFP and C-terminal pAcGFP-PLP. The resulting plasmid constructs were propagated by standard procedure and purified using maxi prep Plasmid Kit (Qiagen, USA). Orientation of the cDNA insert was confirmed by restriction mapping and DNA sequencing (Applied Biosystems). Transfection of these constructs into COS7 cells and positive immunostaining with PLP specific antibodies, including live staining with the O10 antibody (Jung et al., 1996), confirmed translation and correct insertion of PLP into the plasma membrane. -10 and -20 N-termini amino acid deletion mutants were generated by touch up PCR amplification of PLPcDNA containing plasmid pDM100.68. Primers with N-termini 10 and 20 amino acid deletions were designed with the N-terminus methionine intact, and the product was sub-cloned into Egfp-N1 at the EcoRI and Bam HI restriction sites. Mutant clones were confirmed by sequencing. Cycling conditions were 95°C for 1 min, 95°C for 50 sec, 48°C for 1 min, 68°C for 1 min for 3 cycles by 58°C for 25 cycles.

In vitro co-localization of PLP to mitochondria. COS7 cells were cultured in DMEM (Gibco BRL) supplemented with 10% fetal bovine serum (Gibco BRL) with antibiotics. All transient transfections were done using this non-glial cell line and performed when the cells were 70% confluent using Lipofectamine 2000 with approximately 500ng-1μg cDNAs for approximately 4 hrs. The constructs utilized were all driven by CMV: N-terminal EGFP full-length PLP fusion protein, EGFP, P0 (courtesy of J. Kamholz, Wayne State University), Na^+ channel subunit 1 (courtesy of L. Isom, Univ. of Michigan), PMP22 (courtesy of G. Snipes, Baylor University) and CK-YFP (courtesy of M. Hüttemann). Cells were rinsed and grown for an additional 24 or 48 hrs. Mitochondria were stained live with Mitotracker Red 580 (Molecular Probes). Cells were imaged on a Zeiss Apotome Fluorescent Microscope (Axio Vision 4.7.lnk), images were deconvolved using Huygens Essential Software (Scientific Volume Imaging B.V.) and compiled in Adobe Photoshop. In the co-transfection studies COS7 cells were co-transfected with wild-type PLP-EGFP and wild-type CK-YFP allowed to grow for 24 to 48 hrs, stained live with Mitotracker Red 580, fixed and analyzed by confocal fluorescent microscopy using the Leica TCS SP5 (LASAF8.1.1), and images were processed as described above.

Electron microscopy. We quantified the area occupied by mitochondria in Olgs of *Plp1*tg, jp, and their appropriate controls. Mice were perfused intracardially with 4% formaldehyde prepared from paraformaldehyde or with addition of 0.5% glutaraldehyde (Electron Microscopy Sciences, Hatfield PA). Corpora callosa and striata from 35 to 45 day *Plp1*tg (n=3), and age-matched controls (n=2) and 15-17 day postnatal jp mice (n=2) were thin-sectioned. Beginning in the center of a grid and working outwards, all cells with moderate to dense cytoplasm were photographed until about 50 cells were photographed. After development, cells were classified as Olgs, microglia, astrocytes, or unclassifiable because of too little cytoplasm. Approximately 25 Olgs per mouse

were digitized for quantification. The perimeter of the plasma membrane and nucleus was outlined with Image J (NIH), and cytoplasmic area obtained for each cell by subtracting nuclear from total cellular area. For these same cells, the number of mitochondria was calculated; their areas were outlined and summed. The numbers and area of the mitochondria was calculated as a percentage of the cytoplasmic area.

Post-embedding immunogold electron microscopy. Thirty to 50 day old *Plp1*tg mice were perfused with 4% paraformaldehyde and 0.5% glutaraldehyde, brains dissected and 1mm x 3mm blocks embedded in LR White (London Resin Company Ltd., Berkshire England) following their protocol. Ultra-thin sections were cut and mounted on 200 mesh nickel grids. A PLP antibody to the carboxy terminus diluted 1:500 in PBS was applied overnight, grids rinsed, and secondary goat anti-rabbit antibody conjugated to 12nm gold particles (Jackson ImmunoResearch Laboratories, Inc. West Grove, PA) was applied for 2 hrs, sections rinsed, air dried, and lightly stained with uranyl acetate and lead citrate. Thin sections were systematically scanned for Olg perikarya, photographed, and then astrocytes and neurons in closest proximity to the oligodendrocytes were photographed. The striatum and corpora callosa were imaged on a JEOL 1010 electron microscope, negatives scanned into Adobe Photoshop and printed for analyses. Both the number of mitochondria and the number of gold particles overlying mitochondria were counted in different cell types (Olgs, astrocytes, neurons and their processes). The assumption is that PLP is not present in mitochondria of cells; therefore, any increase in the percentage of mitochondria with gold particles in a certain type of cell indicates specific localization. The percentage of mitochondria overlain with gold particles was counted for each cell type in *Plp1*tg. The post-embedding PLP immuno-gold staining procedure was repeated by another laboratory (Dr. Holt at WSU) using different *Plp1*tg mice with similar findings.

RESULTS

The levels of ATP in whole brain homogenates of *Plp1*tgs and jp mice were compared to their appropriate controls (Figure 1). *Plp1*tgs were 30-35 days old; their phenotype was manifested by tremors and tonic-clonic seizures; their genotype was confirmed by the presence of a transgene and/or qPCR of the *Plp1* gene. Because jp male mice die between 19 and 22 days, we studied them and their age-matched controls at 17-19 days. Both sets of mice were starved for 5-6 hrs to provide a well-defined metabolic state for controlled mitochondrial studies (Lee et al., 2005). Strikingly, *Plp1tg* mice have a 50% reduction in ATP levels whereas jp mice have normal levels. The ATP reduction in *Plp1*tgs demonstrates a severely compromised energetic state, suggesting major mitochondrial dysfunction. Overnight starvation, which has no apparent effect on wild-type mice, often resulted in death of *Plp1*tg mice, indicating that these animals not only have a severely compromised energy homeostasis but that food must constantly be provided to compensate for their acute energy deficit.

To determine whether the respiratory chain has intrinsic deficits, we examined a key mitochondrial enzyme, cytochrome *c* oxidase (CcO). CcO is the terminal enzyme of the mitochondrial respiratory chain (complex IV) and consumes more than 90% of cellular oxygen. Overall mitochondrial respiration is tightly coupled to CcO, and CcO is

the proposed pacemaker of oxidative metabolism in intact cells (Villani et al., 1998; Villani and Attardi, 2000). In order to determine the range of activities in which CcO operates, allosteric regulation through ATP (an allosteric inhibitor that operates under conditions of sufficient cellular energy) and ADP (an allosteric activator that operates under conditions when ATP is utilized and converted into ADP) has to be considered and analyzed. We measured CcO activity of *Plp1*tg, jp and control mice in the presence of 5mM ATP and an ATP regenerating system or 5mM ADP. Ex vivo CcO activities are similar in *Plp1*tg and jp mice when compared to their controls (Figure 2). This finding suggests that oxidative phosphorylation is not intrinsically altered in both mutants. This ex vivo result does not mean the mitochondrial defect is not detectable in brain homogenates due to the fact that Olgs represent only a minor fraction of brain cells. In vivo CcO activity should still be increased because its activity and O_2 consumption are allosterically regulated through the ratio of ATP (inhibitor) and ADP (activator). A 50% reduction in ATP and a concomitant increase in ADP should lead to full allosteric activation assuming that total adenine nucleotide concentration is not dramatically changed in the *Plp1*tg animals. The resulting increased aerobic activity may explain increased substrate (food) demand and thus the striking effects on the overnight starved *Plp1*tg mice.

CcO histochemistry. CcO activity is directly measurable on brain sections using a histochemical technique (Wong-Riley, 1979). This method assesses CcO function in a more physiological context since the cellular environment is present and mostly intact. Densitometric sampling of CcO reaction product in white and grey matter of mice starved for 5-6 hrs revealed an average increase of 10% throughout the cerebrum of *Plp1*tg mice (Table 1). While the increase is greatest in white matter, the grey matter also shows increases, especially the hippocampus. The smaller than expected changes in CcO histochemical reactivity are in line with other studies that show 10-30% increases in reactivity in diseases with oxidative metabolic disorders (eg., Wong-Riley et al., 1997). The modest changes found with this technique may also be due to the methodology that dilutes cellular components, including ATP and ADP (Hüttemann et al., 2007). These values may underestimate the role of allosteric regulation via the ATP/ADP ratio.

Histochemical density analysis of grey matter includes mainly neuronal components, suggesting neurons are somehow involved. Interestingly, scattered neurons in *Plp1*tg striatum and hippocampus show noticeable increases in histochemical staining compared to the most intensely stained neurons in controls. This finding strongly suggests that metabolism is compromised not only in Olgs but also in neurons. Given the 50% reductions in ATP in *Plp1*tg brains, oxidative phosphorylation deficiencies in many neural cell types might be predicted.

Mitochondrial membrane potential ($\Delta\Psi_m$). $\Delta\Psi_m$ is generated by the electron transport chain complexes including CcO that pumps protons across the inner mitochondrial membrane (IMM). Depolarization of $\Delta\Psi_m$ is detectable with voltage dependent probes including JC-1 (5,5', 6,6'-tetrachloro-1,1',3,3' tetraethylbenzimidazolyl-carbocyanine iodide). JC-1 exists as a green monomer at low membrane potentials and accumulates as a red aggregate in mitochondria around normal membrane potentials (Lugli et al.,

2007). We first examined $\Delta\Psi_m$ in COS7 cells transiently transfected with a full-length cDNA PLP-EGFP, a full-length cDNA P0-EGFP, a full-length PMP-22-EGFP, a full-length Na^+ channel β-subunit-EGFP, and a LacZ-EGFP. Cells with a normal $\Delta\Psi_m$ exhibit many red punctate ellipsoids in their cytoplasm. With all constructs, mitochondria in COS7 cells are mainly perinuclear (Figure 3). Eight-12 hrs after transfection with PLP-EGFP, COS7 cells show low levels of PLP and many red mitochondria (Figure 3A-B). Twenty-four hrs after transfection, COS7 cells exhibit higher levels of PLP and exhibit little or no red fluorescence in their cytoplasm. Non-transfected cells on the same coverslip produce red fluorescent mitochondrial signals indicating their $\Delta\Psi_m$ is normal. (In the PLP transfected cells, EGFP and the JC-1 monomer in mitochondria are excited at nearly the same wavelength, making it difficult to distinguish between depolarized mitochondria and PLP-EGFP). Cells transfected with P0, PMP-22, Na^+ channel β-subunit, or LacZ constructs (Figure 3 C-H) show red fluorescent mitochondria similar to untransfected cells. The pictures chosen here illustrate low and high level expression of these plasma membrane proteins to demonstrate that even in cells expressing high levels of proteins, mitochondria stain red. Therefore, over-expression of plasma membrane proteins that leads to intense GFP fluorescence in the cytoplasm does not necessarily cause mitochondrial depolarization.

We next compared $\Delta\Psi_m$ in brain slices from age-matched *Plp1*tg, jp, and wild-type mice (Figure 4). Transverse slices of cerebrum were incubated with JC-1 dye in buffer within 5 minutes of removing their brains, imaged within two minutes after rinsing the dye, and images deconvolved at a later time. We quantified the ratio between red (mitochondria with normal $\Delta\Psi_m$) and green (mitochondria with lowered $\Delta\Psi_m$). While mitochondria with lowered $\Delta\Psi_m$ are abundant in all 3 preparations and likely reflect O_2 depletion due to time lag in imaging, differences between *Plp1*tg mice with wild-type and jp mice are dramatic. The ratio of red to green fluorescent signal for 35-day *Plp1*tg mice is significantly reduced 2.5-fold. The ratio of red to green fluorescent signal for 15-17 day jp mice is slightly increased compared to 15-17 day control mice. (Figure 4E). Thus, mitochondria in jp exhibit values similar to controls, even though a larger percentage of Olgs are dying in jp than in *Plp1*tgs (Cerghet et al., 2001). The hypopolarization of *Plp1*tg mitochondria versus the modest hyperpolarization of jp mitochondria is relevant to the extensive apoptosis in jp. Hyperpolarized mitochondria lead to production of increased free radicals, a crucial signal for apoptosis. Since *Plp1*tg mitochondria have depolarized membrane potentials, it is unlikely they use the same apoptotic pathway as jp.

Mitochondrial abnormalities in vivo. The functional in vivo studies described above suggest that Olg mitochondria in *Plp1*tg mice might differ morphologically from wild-type and jp mice. We quantified the number of mitochondria per square millimeter of cytoplasm in *Plp1*tg mice and compared their numbers to wild-type and jp mice (Figure 5A). Compared to wild-type mice and jp mice, the density of mitochondria in *Plp1*tg Olgs is more than two times greater than controls. In contrast, the density of mitochondria in jp follows the same linear regression line as wild-type Olgs. When the total surface area of Olg mitochondria is plotted versus their cytoplasmic surface area, *Plp1*tg Olg mitochondria occupy more than two-fold the area of wild-type mice (Figure 5B). Interestingly, the surface area for Olg mitochondria in wild-type mice hovered around

7% with little standard error suggesting tight regulation of their numbers. In contrast, Olgs in *Plp1*tg mice exhibited extreme morphological variations. In many Olgs, the cytoplasm is filled with mitochondria (Figure 6). Other Olgs are morphologically similar to their normal counterparts, have a normal distribution of mitochondria, and are often associated with thin myelin sheaths, suggesting they are newly generated and express low levels of PLP. We have found increased generation of new glia throughout the lifespan of these animals, some of which we have confirmed as microglia (Tatar et al., unpublished data) and others possibly Olgs. In addition to the differences in density of mitochondria between *Plp1*tg and control mice, the mitochondria in *Plp1*tg mice appear to be structurally abnormal. High magnification pictures of silver-gold sections of mitochondria show disruptions of the outer mitochondrial membrane (OMM). Often, rough ER appears fused to the OMM. Fission of mitochondria and OMM integrity is associated with apoptosis, loss of $\Delta\Psi_m$, and AIF translocation (Frank et al., 2001).

Association of PLP with Mitochondria. We transfected an N-terminal EGFP full-length PLP construct, a C-terminal GFP full-length PLP construct, a N-terminal EGFP full-length P0 construct, a N-terminal EGFP full-length PMP22 construct, a N-terminal EGFP full-length Na^+ channel β-subunit, and EGFP by itself into COS7 cells, and then labeled mitochondria with Mitotracker Red 580. Cells were fixed at 12-hr intervals up to 48-hrs after transfection. Twelve hrs after transfection, COS7 cells expressing GFP-PLP or PLP-EGFP show little co-localization of PLP with mitochondria (Figure 7A). Between 24-48 hrs after transfection, extensive co-localization is present throughout the cytoplasm (Figure 7B-C).

Deconvolution of confocal images exhibits better resolution and reveals specificity of the co-localization. Both confocal and deconvolved images show only green fluorescence (PLP) in the plasma membrane, indicating Mitotracker Red 580 dye does not bleed into green fluorescent channel (Figure 7D-G). Second, the green, orange-yellow and red profiles associated with mitochondria imaged are often composed of three distinct elements. An all green EGFP crescent partially surrounds an all yellow structure that sometimes encloses an all red mitochondrial component. The green is most likely ER that contains PLP adjacent to mitochondria, the yellow component is most likely the OMM and/or IMM containing PLP, and the red staining a portion of a mitochondrium that lacks PLP. Simultaneous co-transfection of PLP and mitochondrial creatine kinase (mtCK), an IMM-associated protein (Speer et al., 2005), followed by Mitotracker Red 580 staining strongly suggests PLP's insertion into the IMM (Figure 7H-M). Mitotracker Red 580 and mtCK fluorescence co-localizes, as predicted, only in the core of the mitochondria whereas the outer mitochondrial envelope only stains red (Figure 7H-J). PLP co-localizes with Mitotracker Red (Figure 7K-L) and mtCK (Figure 7L-M) to produce yellow variants. The co-localization of PLP to mitochondria is not restricted to COS7 cells as studies performed with an immortalized Olg cell line (Ghandour et al., 2002) into which PLP-EGFP is transfected also shows PLP co-localizes to mitochondria (Figure 7N-P). In contrast to COS7 cells in which most mitochondria show co-localization with PLP, some mitochondria in these Olgsshow strong co-localization whereas others show no co-localization.

Because the N-terminus of PLP contains motifs for localization to the IMM (see Discussion), we made deletions of the first 10 and 20 amino acids that retain the first

amino acid methionine. These constructs show PLP does not co-localize to mitochondria (Figure 8A-F). Faint PLP-EGFP staining is detectable at the plasma membrane indicating modest transport of these mutant constructs. Not surprisingly, live immunostaining with the O10 antibody (Jung et al., 1996) shows the mutants are not correctly inserted into the plasma membrane. The specificity of PLP's co-localization with mitochondria is confirmed by transfection of other plasma membrane markers and Mitotracker Red 580 staining. The myelin plasma membrane protein P0, when transfected into COS7 cells, does not co-localize with mitochondria (Figure 9A-C); PMP22, another Schwann cell plasma membrane protein, does not co-localize with mitochondria (Figure 9D-F). Cells transfected with EGFP alone exhibit very bright nuclear and cytoplasmic staining but little co-localization with mitochondria (data not shown). The intensity of the EGFP signal in these P0 and PMP-22 transfected COS7 cells is as intense as in the PLP-EGFP or GFP-PLP cells, indicating that over-expression of myelin plasma membrane proteins does not necessarily lead to their co-localization in mitochondria.

Because ER and mitochondria are structurally in close proximity to each other, it might be argued that the yellow mitochondrial fluorescence observed with PLP-EGFP or GFP-PLP constructs and Mitotracker Red is due to fluorescence bleed through from ER into mitochondria or that the two organelles overlap each other in the z-axis. However, live Mitotracker Red 580 staining and anti-KDEL (an endoplasmic reticulum marker) antibody immunostaining show very little co-localization (Figure 9G-I).

We next asked whether PLP co-localized with mitochondria in vivo using immunoblots and immunogold EM. We first prepared whole spinal cord and brain homogenates, cytosol, and mitochondrial fractions from 60 day wild-type and *Plp1*tg mice. Immunoblots were probed with a PLP specific antibody, stripped and re-probed with different organelle and plasma membrane markers. Pure mitochondrial fractions were more easily purified from spinal cord (Figure 10A) than from brain. Spinal cord homogenate containing myelin and cytosolic fractions from wild-type and *Plp1*tg mice predictably immunostained for PLP. Approximately 5x less homogenate was loaded compared to the other fractions because the homogenate contains myelin membranes. The intensity of the homogenate bands shows the abundance of myelin proteins in membranes. Mitochondrial fractions from wild-type mice did not show PLP bands but they were easily detectable in *Plp1*tg mice. Its absence in wild-type mice is not a loading artifact because actin levels are approximately equal in both wild-type and *Plp1*tg mitochondrial fractions. The specificity of the mitochondrial fractions was shown with different antibodies. The subunit of CcO, which is coded by mitochondrial DNA and localized to the mitochondrial membrane is restricted to mitochondria and absent in cytosolic fraction. Contamination of mitochondria with other cytosolic organelles was eliminated by probing for ER, Golgi, and lysosomal markers. Two plasma membrane markers, a pan Na^+ channel and the NG2 antibody that recognizes a proteoglycan on glial progenitors, were also, predictably, absent from mitochondrial fractions. Because of the high molecular weights of the last 2 antibodies, they were run on a separate gel but the same sample was used for both blots. We also used MBP as a potential control for the purity of the mitochondrial fractions but, unfortunately, MBP is drastically reduced in the transgenics, making this protein a less than ideal control. In C57 mice, all 4 myelin basic protein (MBP) isoforms were abundantly present in homogenates and faintly

present in the cytosolic fraction whereas only the 21.5kD was detectable in the *Plp1*tg cytosolic fraction (Figure 10B). Drastic reductions of MBP, using immunostaining and Western blotting of total brain homogenates, have been observed by our and other laboratories (Readhead et al., 1994; Karim et al., 2007). While all MBP isoforms were absent in *Plp1*tg mitochondrial fraction (Figure 10B), PLP and DM20 were detected in the mitochondrial fraction of *Plp1*tg mouse. Their MW's were slightly lower than in homogenates but this result is predicted if these proteins are inserted into mitochondria (see Discussion). (The MW of PLP in the mitochondrial fraction in Figure 10A appears slightly lower than in the cytosolic fraction; the obvious difference in MWs in the lower versus the upper blot may be due to the length of time the gel was run).

We next investigated whether PLP localizes to mitochondria in *Plp1*tg mice using pre-and post-embedding immunogold electron microscopy (EM) (Figure 11). With pre-embedding EM immunocytochemistry, penetration was very limited, about 0.25μm from the surface of the tissue block, so very few Olgs were located and detected. This technical problem prevented reliable quantification. Still, the few Olgs near the tissue surface had abundant gold particles overlying their mitochondria whereas mitochondria in other cells lacked gold particles. With the post-embedding method, quantification of the number of gold particles overlying Olg mitochondria showed a several-fold increase compared to the number of gold particles in mitochondria of astrocytes and neurons immediately adjacent to the Olgs (Table 2). The appropriate control for this study is to compare numbers of gold particles in mitochondria of Olgs to adjacent non-Olg cells in the same section. With EM immunogold post-embedding method, the background (random gold particles) varies considerably from animal to animal and even, we find, one side of the grid to the other. This variability is due to several factors and includes differences in penetration of the primary antibody into the plastic. This in vivo EM data, combined with Western blotting and transfection experiments indicates that native PLP co-localizes with mitochondria.

DISCUSSION

Pelizaeus-Merzbacher Disease is due to different types of mutations in the *Plp1* gene. Disabilities range from severe motor impairment and cognitive loss to mild forms in which patients ambulate and have near normal lifespans (Garbern et al., 1999; Woodward, 1999; Regis et al., 2005). Future therapies to treat PMD hinge upon understanding the molecular and cellular sequence of events that contribute to behavioral disabilities. *Plp1* transgenic mouse line 66 closely mimics PMD patients with duplications and triplications of the native gene because the mice we use have mainly duplications, triplications, and quadruplications of the native PLP1 gene. They both have modest increases in proteolipid protein (Supplemental Figure 2; Anderson et al., 1998; Karim et al., 2007), and exhibit a behavioral phenotype similar to PMD patients (see Experimental Procedures).

Hallmarks of all *Plp1* mutations at the histological level are varying degrees of dys-, hypo-, and demyelination accompanied by Olg death. The failure to form myelin is a direct consequence of Olg death rather than a feedback mechanism in which abnormal myelin formation triggers Olg death (Skoff and Knapp, 1990; Skoff, 1995; Yang and Skoff, 1997). An unfolded protein response (UPR) has been studied in

rodents with missense/nonsense mutations and in Olgs cultured from *Plp1* mice with duplications (Southwood et al., 2002; Dhaunchak and Nave, 2007; Southwood et al., 2007) because an UPR is a likely candidate to activate cell death pathways (Harding et al., 2002). An UPR is easily demonstrated in mice with point mutations such as jp, myelin synthesis deficient, and rumpshaker but markers of an UPR are, at best, slightly increased in mice with duplications compared to wild-type mice (Cerghet et al., 2001). Also, markers of cell death pathways in these two groups of mutants were different; the data suggests that the caspase-dependent pathway was activated in mice with missense mutations and the caspase-independent pathway was activated in mice with *PLP1* duplications (see Introduction).

We first studied ATP levels in brains of *Plp1*tg and jp brains and found dramatic differences. ATP levels are drastically reduced in *Plp1*tgs but normal in jp. Concomitant with ATP reduction in the *Plp1*tgs, $\Delta\Psi_m$ is severely reduced in both white and grey matter compared to controls but not in jp. Predictably, CcO, the terminal enzyme in oxidative phosphorylation, was modestly increased in *Plp1*tgs using a histochemical stain. Fifty percent reductions in ATP, dramatic decreases in $\Delta\Psi_m$, and increases in CcO activity throughout white and grey matter make it difficult to attribute these metabolic differences exclusively to Olgs. The reason is that Olgs constitute a small volume of brain tissue. However, energetic coupling between brain cells has been reported and may explain our observed global energy defects. Via the so-called astrocyte-neuron lactate shuttle, astrocytes metabolize glucose to lactate that is secreted and taken up by neurons to drive aerobic energy production (Kasischke et al., 2004). Such an energetic coupling could be a more generalized mechanism in the brain that involves additional participants including Olgs.

Our $\Delta\Psi_m$ measurements sampled grey matter as well as white matter, making it highly likely that neurons were included in these measurements. Large cells, undoubtedly neurons, show stronger CcO staining in striatum of *Plp1*tgs than in controls. The suggestion that neurons in *Plp1*tgs are metabolically abnormal may be paradoxical considering the mutation is expressed in Olgs and not in neurons. However, axonal degeneration in these same *Plp1*tg mice has been previously described (Anderson et al., 1998) indicating that the PLP mutation affects neuronal function.

Our previous studies and the present study now shed light upon the neuronal abnormalities. We found global, large decreases in pH of *Plp1*tg brains (Skoff et al., 2004a) and in stably transfected PLP expressing cells (Boucher et al., 2002). When PLP but not DM20 or control cells were co-cultured with dorsal root ganglion neurons, axonal and neuronal degeneration was striking in these co-culture experiments. These results are not a tissue culture phenomenon because a time-lapse proton-flux ex vivo assay revealed the pH of buffer derived from *Plp1*tg brains was significantly decreased compared to wild-type brains (Skoff et. al., 2004a). These studies suggest that PLP modulates neural dysfunction/death by regulation of pH in vitro and in vivo. The level of PLP regulates the number of Olgs in roughly inverse proportions. The number of Olgs cultured in the presence of antisense PLP was increased as much as seven-fold compared to Olgs grown in control conditions (Yang and Skoff, 1997). The number of Olgs cultured from *Plp1* knockout mice was two-fold greater than in wild-type mice (Skoff et al., 2004b). Over-expressing DM20, an isoform of PLP, "knock-in" mice (Stecca et al., 2000; Spörkel et al., 2002) have near-normal lifespans compared to

shortened lifespans of different over-expressing PLP mouse lines (Mastronardi et al., 1993; Kagawa et al., 1994; Readhead et al., 1994; Bradl et al., 1999).

Our studies demonstrate that transfection of native PLP causes PLP to intercalate into mitochondria, presumably into the IMM. Mitotracker Red 580 staining combined with transfection of CK, located in the IMM, shows oval shaped mitochondria enclosing a classically shaped IMM/matrix. When PLP is transfected into the above combination, PLP co-localizes with CK. Importantly, the co-localization of PLP with mitochondria is not due to "over-expression" of PLP in COS7 cells and immortalized Olg cells such that the protein associates non-specifically with mitochondria. We have "over-expressed" several different plasma membrane proteins such that their level of fluorescence was similar and as bright as that for the PLP expressing cells yet these proteins did not co-localize with mitochondria.

A genome-wide bioinformatics screen and localization prediction programs did not predict PLP to be a tail-anchored mitochondrial protein (Nakai and Horton, 1999; Guda et al., 1994; Kalbfleisch et al., 2007) but this may be due to the high-stringency parameters applied. The absence of a canonical mitochondrial targeting sequence for PLP is not surprising because, if there were one, PLP would be exclusively targeted to mitochondria and not to myelin. Other analyses suggest that PLP is targeted to OMM and/or IMM. It is important to discuss this information in some detail because it lays the theoretical foundation for our co-localization studies. For tail anchoring into the OMM a positively charged C-terminus is required (Horie et al., 2002; Habib et al., 2003) which is present in PLP (267-LKLMGRGTKF-276). The requirements for insertion into the OMM are a relatively short C-terminus with a hydrophobic trans-membrane sequence (TMS) that for PLP includes 21 of 28 amino acids in the fourth TMS. All myelin proteins do not exhibit these C-termini features; P0, for example, which has nearly 70 amino acids in its C-terminus, is an unlikely candidate and did not show co-localization to mitochondria. Similarly, PMP22 and a Na^+ channel β-subunit did not co-localize with mitochondria in transfection studies nor was MBP present in the mitochondrial fractions. Taken together, these studies indicate that the localization of PLP to mitochondria is specific to this myelin membrane protein.

For protein localization to the intermembrane space, a redox-coupled pathway was recently discovered that involves a redox chain consisting of Erv1, Mia40, and cytochrome *c* (Allen et al., 2005). Proteins imported by this pathway usually contain a twin Cx_3C or Cx_9C motif that are oxidized by Mia40 to form disulfide bonds that can trap proteins in the mitochondrial inter-membrane space. PLP contains single Cx_3C and Cx_9C motifs in the N-terminal region, in addition to a Cx_8C sequence located toward the C-terminal part. Other proteins with disulfide bonds that localize to this sub-mitochondrial compartment do not follow this strict rule (Gabriel et al., 2007; Herrmann and Kohl, 2007). Another recently described internal signal for protein localization involves the four amino acid core sequence AVPI together with a matrix-targeting signal that, if present, is sufficient to localize proteins to the inter-membrane space (Ozawa et al., 2007). PLP contains a similar four amino acid motif (171-AVPV-174) where the terminal isoleucine is replaced by valine, which only differs by the absence of a methyl group.

Another algorithm, which predicts the probability of membrane protein insertion into the mitochondrial matrix, shows PLP has an 18% probability for insertion into the mitochondrial matrix (Claros and Vincens, 1996). Insertion into the IMM requires, amongst other factors, an N-terminal cleavable pre-sequence which, for PLP, might be between the 19th and 20th amino acid. This N-terminal leader sequence usually forms an amphipathic helix that contains non-polar amino acids in addition to positively charged residues, clustered on one side. Interestingly, our Western blots show the molecular weight of PLP/DM20 in the mitochondrial fractions is slightly less than in the homogenates and cytosolic fractions.

Partial localization or translocation to mitochondria of plasma membrane and cytoplasmic proteins has been described, providing a basis for PLP, a plasma membrane, insertion into mitochondria. The mammalian protein Slit3 localizes to both cell surface and mitochondria (Little et al., 2001), and tyrosine phosphatase Ship2 localizes to the cytoplasm and mitochondrial intermembrane space (Salvi et al., 2004). Proteins also translocate to mitochondria under certain conditions that include the EGFR receptor where it interacts with CcO subunit II (Boerner et al., 2004) and Akt after activation of the pathway (Bijur and Jope, 2003). Localization and insertion of PLP into the IMM could account for the observed $\Delta\Psi_m$ depolarization and decreased energy levels. In this scenario, direct interaction with and inhibition of one or more OxPhos complexes or through generation of a pore would directly dissipate $\Delta\Psi_m$ similar to uncoupling protein 1 that operates in brown adipose tissue (Brand et al., 1999). The co-localization of PLP with CK strongly supports its association with IMM.

The reduction in ATP levels and decreased $\Delta\Psi_m$ predicts, as we found, an increase in numbers of mitochondria in Olgs of *Plp1*tg mice compared to wild-type and jp mice. An increase in mitochondria is characteristic of cells with reduced respiratory capacity, perhaps due to increased fission and decreased fusion (Detmer and Chan, 2007). The increase in native *Plp1* gene dosage begs the question of whether it has a role in normal development when message and protein levels are highly up regulated. *Plp1* message and protein are expressed at high levels in interdigital webbing of normal mice where it co-localizes with apoptotic cells (Skoff et al., 2004a). In the testes, when PLP/DM20 message is abundant, apoptotic cells are increased in *Plp1*tg mice but decreased in PLP null mice, indicating PLP modulates apoptosis in many cell types. Whether PLP associates with mitochondria in these conditions remains to be studied. Most importantly, our findings of ATP reductions are directly relevant to PMD patients with duplications. Drugs that operate through a variety of direct and indirect mechanisms to prevent reduction of ATP and/or development of gene therapy to reduce *Plp1* expression levels should be feasible candidates to treat PMD patients.

ACKNOWLEDGEMENTS: The authors thank Lori Isom at University of Michigan MI for the Na+ channel β subunit EGFP, John Kamholz at Wayne State University MI for the P0-EGFP construct, G. Jackson Snipes at Baylor University TX for the PMP22-EGFP construct, Alison Fannon at Mt. Sinai School of Medicine NY for the DM20 cDNA, Anthony Campagnoni at UCLA for the PLP cDNA, Said Ghandour, at CNRS Strasbourg France for the immortalized Olg cell lines, Carol Readhead at Cedars-Sinai CA for the *Plp1* transgenic mice, and James Hatfield, VA Medical Center, Detroit MI. for assistance in immunogold electron microscopy.

FUNDING: This research was supported by NIH NINDS NS38236 and European Leukodystrophy Association to RPS.

REFERENCES

Allen S, Balabanidou V, Sideris DP, Lisowsky T, Tokatlidis T (2005) Erv1 mediates the Mia40-dependent protein import pathway and provides a functional link to the respiratory chain by shuttling electrons to cytochrome *c*. J Mol Biol 353:937-944.

Anderson TJ, Schneider A, Barrie JA, Klugmann M, McCulloch MC, Kirkham D, Kyriakides E, Nave KA, Griffiths IR (1998) Late-onset neurodegeneration in mice with increased dosage of the proteolipid protein gene. J Comp Neurol 394:506-519.

Bijur GN, Jope R S (2003) Rapid accumulation of Akt in mitochondria following phosphatidylinositol 3-kinase activation. J Neurochem 87:1427-1435.

Boerner JL, Demory ML, Silva C, Parsons SJ (2004) Phosphorylation of Y845 on the epidermal growth factor receptor mediates binding to the mitochondrial protein cytochrome c oxidase subunit II. Mol Cell Biol 24:7059-7071.

Boespflug-Tanguy O, Mimault C, Melki J, Cavaqna A, Giraud G, Pham Dinh D, Dastuque B, Dautigny A (1994) Genetic homogeneity of Pelizaues-Merzbacher disease: tight linkage to the proteolipidprotein locus in 16 affected families. PMD Clinical Group Am J Hum Genet 55:461-467.

Boucher SE, Cypher MA, Carlock LR, Skoff RP (2002) Proteolipid protein gene modulates viability and phenotype of neurons. J Neurosci 22:1722-1783.

Bradl M, Bauer J, Inomata T, Zielasek J, Nave KA, Lassmann H, Wekerle H (1999) Transgenic Lewis rats overexpressing the proteolipid protein gene: myelin degeneration and its effect on T cell-mediated experimental autoimmune encephalomyelitis. Acta Neuropathol 97:595-606.

Brand MD, Brindle KM, Buckingham JA, Harper JA, Rolfe DF, Stuart JA. (1999) The significance and mechanism of mitochondrial proton conductance. Int J Obes Relat Metab Disor. 23 Suppl 6:S4-S11.

Cerghet M, Bessert DA, Nave KA, Skoff RP (2001) Differential expression of apoptotic markers in jimpy and in Plp overexpressors : evidence for different apoptotic pathways. J Neurocytol 30:841-855.

Claros MG, Vincens P (1996) Computational method to predict mitochondrially imported proteins and their targeting sequences. Eur J Biochem 241:779-786.

Cregan SP, Dawson VL, Slack RS (2004) Role of AIF in caspase-dependent and caspase independent cell death. Oncogene 23:2785-2796.

Detmer S, Chan D (2007) Functions and dysfunctions of mitochondrial dynamics. Nature Reviews/Molecular Cell Biology 8:870-879.

Dhaunchak AS, Nave KA (2007) A common mechanism of PLP/DM20 misfolding causes cysteine-mediated endoplasmic reticulum retention in oliogdendrocytes and Pelizaeus-Merzbacher disease. Proc Natl Acad Sci USA 104:17813-17818.

Ellis D, Malcolm S (1994) Proteolipid protein gene dosage effect in Pelizaeus-Merzbacher disease. Nat Genet 6:333-334.

Frank S, Gaume B, Bergmann-Leitner ES, Leitner WW, Robert EG, Catez F, Smith CL, Youle RJ (2001) The role of dynamin-related protein 1, a mediator of mitochondrial fission, in apoptosis. Dev Cell 1:515-525.

Gabriel K, Milenkovic D, Chacinska A, Müller J, Guiard B, Pfanner B, Meisinger C 2007. Novel mitochondrial intermembrane space proteins as substrates of the MIA import pathway. J Mol Biol 365:612-620.

Garbern JY, Cambi F, Lewis R, Shy M, Sima A, Kraft G, Vallat JM, Bosch EP, Hodes ME, Dlouhy S, Raskind W, Birt T, Macklin W (1999) Peripheral neuropathy caused by proteolipid protein gene mutations. Ann NY Acad Sci 883:351-365.

Garbern JY (2007) Pelizaeus-Merzbacher disease : Genetic and cellular pathogenesis. Cell Mol Life Sci 64:50-65.

Haeberlein SL (2004) Mitochondrial function in apoptotic neuronal cell death. Neurochem Res 29:521-530.

Ghandour M, Feutz A, Jalabi W, Taleb O, Bessert D, Cypher M, Carlock L, Skoff R (2002) Trafficking of PLP/DM20 and camp signalling in immortalized jimpy oligodendrocytes. Glia 40:300-311.

Guda C, Fahy E, Subramaniam S (2004) MITOPRED: a genome-scale method for prediction of nucleus-encoded mitochondrial proteins. Bioinformatics 20:1785-1794.

Habib SJ, Vasiljev A, Neupert W, Rapaport D (2003) Multiple functions of tail-anchor domains of OMM proteins. FEBS Lett 555:511-515.

Haeberlein SL (2004) Mitochondrial function in apoptotic neuronal cell death. Neurochem Res 29:521-530.

Harding HP, Calfon M, Urano F, Novoa I, Ron D (2002) Transcriptional and translational control in the mammalian unfolded protein response. Annu Rev Cell Biol 18:575-599.

Herrmann JM, Kohl R (2007) Catch me if you can! Oxidative protein trapping in the intermembrane space of mitochondria. J Cell Biol 176:559-563.

Hodes ME, Pratt VM, Dlouhy SR (1993) Genetics of Pelizaeus-Merzbacher disease. Dev Neurosci 15:383-394.

Horie C, Suzuki H, Sakaguchi M, Mihara K (2002) Characterization of signal that directs C-tail-anchored proteins to mammalian mitochondrial outer membrane. Mol Biol Cell 13:1615-1625.

Hüttemann M, Lee I, Samavati L, Yu H, Doan JW (2007) Regulation of mitochondrial oxidative phosphorylation through cell signaling. Biochim Biophys Acta 1773:1701-1720.

Hüttemann M, Lee I, Kreipke CW, Petrov T (2008) Suppression of the inducible form of nitric oxide synthase prior to traumatic brain injury improves cytochrome *c* oxidase activity and normalizes cellular energy levels. Neuroscience 151:148-154.

Jung M, Sommer I, Schachner M, Nave K-A (1996) Monoclonal antibody O10 defines a confromationally sensitive cell-surface epitope of proteolipid protein (PLP): evidence tht PLP misfolding underlies dysmyelination in mutant mice. J Neurosci 16:7920-7929.

Kalbfleish T, Cambon A, Wattenberg BW (2007) A bioinformatics approach to identifying tail-anchored proteins in the human genome. Traffic 8:1687-1694.

Karim SA, Barrie JA, McCulloch MC, Montague MC, Montague P, Edgar JM, Kirkham D, Anderson TJ, Nave KA, Griffiths IR, McLaughlin M (2007) PLP overexpression perturbs myelin protein composition and myelination in a mouse model of Pelizaeus-Merzbacher Disease. GLIA 55:341-351.

Kasischke KA, Vishwasrao HD, Fisher PJ, Zipfel WR, Webb WW (2004) Neural activity triggers neuronal oxidative metabolishm followed by astrocytic glycolysis. Science 305:99-103.

Knapp PE, Skoff RP, Redstone DW (1986) Oligodendroglial cell death in jimpy mice : an explanation for the myelin deficit. J Neurosci 6:2813-2822.

Kramer-Albers E-M, Gehrig-Burger K, Thiele C, Trotter J, Nave K-A (2006) Perturbed interactions of mutant proteolipid protein/DM20 with cholesterol and lipid rafts in oligodendroglia: implications for dysmyelination in spastic paraplegia. J Neurosci 26:11743-11752.

Lee I, Bender E, Kadenbach B (2002) Control of mitochondrial membrane potential and ROS formation by reversible phosphorylation of cytochrome *c* oxidase. Mol Cell Biochem 234-235:63-70.

Lee I, Salomon AR, Ficarro S, Mathes I, Lottspeich F, Grossman LI, Hüttemann M (2005) cAMP-dependent tyrosine phosphorylation of subunit I inhibits cytochrome *c* oxidase activity. J Biol Chem 280:6094- 6100.

Little MH, Wilkinson L, Brown DL, Piper M, Yamada T, Stow JL (2001) Dual trafficking of Slit3 to mitochondria and cell surface demonstrates novel localization for Slit protein. Am J Physiol Cell Physiol 281:486-495.

Lugli E, Troiano L, Cossarizza A (2007) Polychromatic analysis of mitochondrial membrane potential using JC-1. Current Protocols in Cytom 7:32:1-15.

McLaughlin M, Karim SAS, Montague P, Barrie JA, Kirkham D, Griffiths IR, Edgar JM (2007) Genetic background influences UPR but not PLP in the rumpshaker model of PMD/SPG2. Neurochem Res 32:167-176.

Nakai K, Horton P (1999) PSORT: a program for detecting sorting signals in proteins and predicting their subcellular localizations. Trends Biochem Sci 24:34-36.

Napiwotzki J, Shinzawa-Itoh K, Yoshikawa S, Kadenbach B (1997) ATP and ADP bind to cytochrome *c* oxidase and regulate its activity. Biol Chem 378:1013-1021.

Ozawa T, Natori Y, Kuroiwa H, Kuroiwa T, Umezawa Y (2007) A minimal peptide sequence that targets fluorescent and functional proteins into the mitochondrial intermembrane space. ACS Chem Biol 2:176-186.

Readhead C, Schneider A, Griffiths I, Nave KA (1994) Premature arrest of myelin formation in transgenic mice with increased proteolipid protein gene dosage. Neuron 12:583-595.

Regis S, Grossi S, Lualdi S, Biancheri R, Filocamo M (2005) Diagnosis of Pelizaeus-Merzbacher disease: detection of proteolipid protein gene copy number by real-time PCR. Neurogenetics 6:73-78.

Salvi M, Stringaro A, Brunati AM, Agostinelli E, Arancia G, Clari G, Toninello A (2004) Tyrosine phosphatase activity in mitochondria: presence of Shp-2 phosphatase in mitochondria. Cell Mol Life Sci 61:2393-2404.

Skoff RP (1995) Programmed cell death in the dysmyelinating mutants. Brain Pathology 5:283-288.

Skoff RP, Knapp PE (1990) Expression of the jimpy phenotype in relation to proteolipid protein appearance. Ann N Y Acad Sci 605:122-134.

Skoff RP, Bessert DA, Cerghet M, Franklin MJ, Rout UK, Nave KA, Carlock L, Ghandour MS, Armant DR (2004a) The myelin proteolipid gene modulates apoptosis in neural and non-neural tissues. Cell Death Differ 11:1247-1257.

Skoff RP, Saluja I, Bessert D, Yang X (2004b) Analysis of proteolipid protein mutants show levels of proteolipid protein regulate oligodendrocyte number and cell death in vitro and in vivo. Neurochem Res 29:2095-2103.

Southwood CM, Garbern J, Jiang W, Gow A (2002) The unfolded protein response modulates disease severity in Pelizaeus-Merzbacher disease. Neuron 36:585-596.

Southwood C, Olson K, Wu CY, Gow A (2007) Novel alternatively spliced endoplasmic reticulum retention signal in the cytoplasmic loop of Proteolipid Protein-1. J Neurosci Res 85:471-478.

Speer O, Back N, Buerklen T, Brdiczka D, Koretsky A. Wallimann T, Eriksson O (2005) Octameric mitochondrial creatine kinase induces and stabilizes contact site between the inner and outer membrane. Biochem J 385:445-450.

Thomson CE, Montague P, Jung M, Nave K-A, Griffiths IR (1997) Phenotypic severity of murine Plp mutants reflects in vivo and in vitro variations in transport of PLP isoproteins. Glia 20:322-332.

Villani G, Greco M, Papa S, Attardi G (1998) Low reserve of cytochrome *c* oxidase capacity in vivo in the respiratory chain of a variety of human cell types. J Biol Chem 273:31829-31836.

Villani G, Attardi G (2000) In vivo control of respiration by cytochrome *c* oxidase in human cells. Free Radic Biol Med 29:202-210.

Wong-Riley M (1979) Changes in the visual system of monocularly sutured or enucleated cats demonstrable with cytochrome oxidase histochemistry. Brain Res 171:11-28.

Wong-Riley M, Antuono P, Ho KC, Egan R, Hevner R, Liebl W, Huang Z, Rachel R, Jones J (1997) Cytochrome oxidase in Alzheimer's disease: biochemical, histochemical, and immunocytochemical analysis of the visual and other systems. Vision Res 37:3593-3608.

Woodward K, Malcolm S (1999) Proteolipid protein gene: Pelizaeus-Merzbacher disease in humans and neurodegeneration in mice. Trends Genet 15:125-128.

Yang X, Skoff RP (1997) Proteolipid protein regulates the survival and differentiation of oligodendrocytes. J Neurosci 17:2056-2070.

FIGURE LEGENDS

Figure 1. ATP levels (% relative to control; 100% is equivalent to 43 μM ATP/mg solubilized protein) were measured with the bioluminescence assay (Roche) in 30-35 day old *Plp1*tg mice, age and strain matched controls, 17-19 day old jp/Ta mice, and age matched littermate controls (+/+). All mice were starved 5-6 hrs. SEM is based on three separate experiments. P<0.0035 for *Plp1*tgs, P>0.05 for jpTa compared to +/+ controls. Paired t-test.

Figure 2. Cytochrome c oxidase (CcO) activities of mice starved for 5-6 hrs. CcO activity measurements used the polarographic method in the presence of 5mM ATP or ADP by increasing the amount of substrate cytochrome *c*. **A**. Comparison of CcO activities of wild-type (WT, squares, n=3) and *Plp1*tg mice (triangles, n=3) shows no significant difference in CcO activities in the presence of ATP (opens symbols) or ADP (closed symbols). **B**. CcO activities of jp mice (circles, n=5) is indistinguishable from wild-type animals (WT, squares, n=5) in the presence of ATP (opens symbols) or ADP (closed symbols). Turnover = consumed O_2 (μM/min/mg total protein).

Figure 3. JC-1 staining of transiently transfected COS7 cells. **A, E**. Cells transfected with wild-type PLP fused to EGFP 8 hrs afterwards show abundant red stained mitochondria in cells expressing moderate levels of PLP. **B, F**. Twenty-four hrs after transfection with wild-type PLP-EGFP, most transfected cells express high levels of PLP and have abnormally low $\Delta\Psi_m$ indicated by loss of red stained mitochondria. Untransfected cells (arrows) show abundant red stained mitochondria indicative of normal $\Delta\Psi_m$ **(F)**. **C, G**. Cells transfected with myelin P0 protein **(C)** or PMP-22 **(G)** fused to EGFP show many red stained mitochondria, even in cells expressing high levels of EGFP. **D, H**. Cells transfected with the β-subunit of Na^+ channel fused to EGFP **(D)** or with LacZ-EGFP **(H)** show many red mitochondria. Arrows indicate non-transfected cells that have mostly red mitochondria. Magnification bar = 10 microns

Figure 4. JC-1 staining of brain striata from strain matched controls **(A-B)** and *Plp1*tg **(C-D)** age-matched mice. One-hundred micron brain slices were stained with JC-1 dye within several minutes of harvesting brains. They were immediately imaged and images de-convolved at a later time. Red ellipsoids indicate relatively normal $\Delta\Psi_m$ and green ellipsoids represent a decrease in potential. Controls have few bright green mitochondria. Notice how "red stained" mitochondria in *Plp1*tgs occupies less area than in controls. Some mitochondria show only red fluorescence (arrows) and others only green fluorescence (arrowheads). **E**. Quantification of red to green ratio. n=number of animals. ***p=0.003, *PLP1*tg compared to wild-type PLP control, t-test.

Figure 5. **A**. The number of mitochondria per mm^2 of Olg cytoplasm is increased more than two-fold in 35 day *Plp1*tg mice compared to both 35 day wild-type and jp mice. Each colored object represents the number of mitochondria contained within the total cytoplasmic surface area of one Olg. **B**. The sum of the mitochondrial area for each Olg was calculated and compared to its total cytoplasmic area. Significant difference of means for t-test: control and *Plp1*tg p<.0001; *Plp1*tg and jp/Ta p<.0001.

Figure 6. Electron micrographs of an Olg from a 35 day wild-type mouse **(A)** and Olgs from a 35 day *Plp1*tg mouse **(B-C)**. Nuclei are outlined in green and mitochondria in pink. The distribution of mitochondria and other organelles from the wild-type mouse is typical of normal Olgs. Although the cytoplasm and nuclei of *Plp1*tg Olgs are abnormally electron dense, their nuclei and plasma membranes are intact, suggesting they are still viable.

Figure 7. A-C. Confocal images of COS7 cells transiently transfected with a full-length PLP-EGFP construct and stained with Mitotracker Red. **A.** 12 hrs after transfection, most mitochondria in transfected cells stain red but some show co-localization with PLP (arrow and inset). Mitochondria in non-transfected cells are all red. **B-C**. By 36 hrs after transfection, co-localization is abundant (arrow and inset). **D-G**. COS7 cells transfected with GFP-full length PLP construct for 36 hrs and live stained for Mitotracker Red. Single channel confocal images **(D-E),** merged **(F),** and deconvolved **(G)** with Huygens Essential Software. **(D-G).** PLP-positive plasma membranes and cytoplasmic organelles (arrowheads) remain green in the merged and deconvolved images; some mitochondria remain red (crossed arrowhead) in the merged and deconvolved images. Co-localization of PLP and mitochondria (arrows) is abundant in merged confocal image. **G.** In the deconvolved image, green staining (PLP) surrounds yellow structures (PLP and mitochondria) that often surrounds a red portion of mitochondria. **H-M**. Confocal images of COS7 cells simultaneously transfected with creatine kinase-YFP and PLP-EGFP and stained with Mitotracker Red 580. **H-J**. Mitotracker Red and creatine kinase, visualized as canary yellow, co-localize as goldenrod **(J)**. A thin rim of red, presumably outer mitochondrial membrane, often surrounds inner mitochondrial membrane localized creatine kinase (arrows). **K-L**. Co-localization of PLP and Mitotracker Red produces yellow-orange staining. PLP (green) often surrounds the matrix localized creatine kinase staining (yellow) (arrows). **M**. Co-localization of PLP (green) and creatine kinase (canary yellow) produces a bright yellow staining. Green surrounds creatine kinase which has a worm-like configuration typical of mitochondrial cristae. **N-P**. Confocal pictures of oligodendrocyte cell line 158N transfected with PLP-EGFP and stained with Mitotracker Red. Single channel confocal images (**N-O)** and merged **(P).** Magnification bar = 10 microns

Figure 8. A-F Confocal pictures of COS7 cells transfected with the first ten **(A-C)** or first 20 **(D-F)** amino acids, exclusive of methionine, deleted from PLP and stained for Mitotracker Red 580. Most mitochondria are red and show no co-localization with PLP. However, faint yellow staining is present in some mitochondria. Truncated PLP is in vesicles that is transported into processes. Magnification bar = 10 microns

Figure 9. A-C. COS7 cells transiently transfected with P0-EGFP and stained with Mitotracker Red 580. **A**. Mitochondria are tubular or round structures spread throughout the cytoplasm but are often aggregated around the nucleus. **B**. P0 forms punctate dots throughout the cytoplasm, large and intensely fluorescent aggregates, and it also outlines the plasma membrane. **C**. In the merged image, mitochondria surrounding the nucleus are not co-labeled with P0 (left arrow); a single mitochondrion near the P0

aggregate (right arrow) is not co-labeled. **D-F**. COS7 cells transiently transfected with PMP22-EGFP and stained with Mitotracker Red 580. PMP22 and P0 do not co-localize with mitochondria in these confocal images except for occasional particles. **G-I**. Confocal, deconvolved images of COS7 cells stained for Mitotracker Red 580, fixed, and immunostained for KDEL using a FITC secondary. Reticulated pattern characteristic of ER (arrows) and tubular mitochondria (crossed arrows) often abut each other but do not co-localize. Close apposition of mitochondria with ER form occasional small dots (arrowheads) but do not show extensive overlap of PLP with mitochondria. Magnification bar = 10 micron

Figure 10. A. Immmunoblots of cytosolic and mitochondrial fractions of spinal cord of 60 day *PLP1*tg and wild-type C57 mice. Mitochondrial and cytosolic fractions were prepared using the Biovision Kit. The immunoblot was first probed with a PLP specific antibody, stripped, and subsequently reprobed for 5 other antibodies. The last 2 antibodies, because of their higher MW's, were run on a gradient gel using the same homogenate. **B.** Immunoblots of whole brain homogenates, cytosolic and mitochondrial fractions probed for PLP and MBP from 60 day C57 and *Plp1*tg mice. Antibody to carboxy terminus of PLP recognizes both PLP and DM20. PLP and DM20 MWs in mitochondrial fraction are slightly less than in whole brain or cytosolic fractions. Antibody to MBP recognizes all 4 MBP isoforms present in homogenate and cytosolic fractions in C57 mice but are absent in mitochondrial fractions. Actin in mitochondrial fraction is always less than in cytosol (see 10A above).

Figure 11. Electron microscopic immunogold sections from 35 day *Plp1*tg mice immunostained for PLP with 10μm gold particles using the post-embedding technique. **A-B.** Nearly adjacent sections show two Olgs with numerous gold particles overlying ribosomes and ER and mitochondria (arrows). Inset shows gold particles overlying mitochondria and a vacuole.

Table 1. Histochemical analysis of CcO in cerebrum from control (n=6) and *Plp1*tg mice (n=6) shows modest increased CcO density in *Plp1*tg (see Results).

Table 2. Ultra-thin sections from 35 day *Plp1*tg corpus callosum and striatum were systematically scanned, all oligodendrocytes and surrounding neuropil were photographed, scanned, and photographically printed (see Fig. 11). All immunogold particles overlying mitochondria were identified with a magnifying loupe and allocated to oligodendrocytes or to mitochondria in all other glia, axons, dendrites, and neuronal perikarya.

ASN NEURO Immediate Publication. Published on 7 August 2009 as manuscript AN20090028

Figure 1

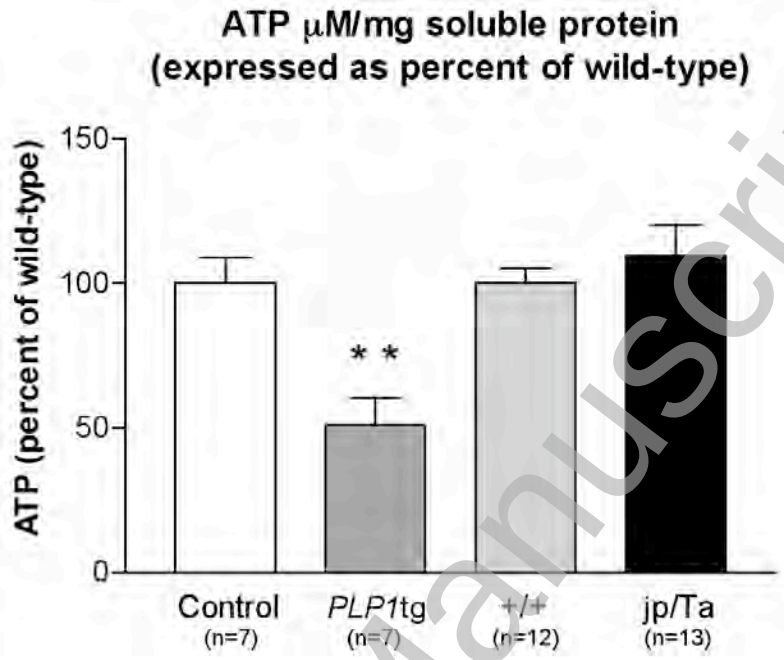

Figure 1. ATP levels (% relative to control; 100% is equivalent to 43 μM ATP/mg solubilized protein) were measured with the bioluminescence assay (Roche) in 30-35 day old *Plp1*tg mice, age and strain matched controls, 17-19 day old jp/Ta mice, and age matched littermate controls (+/+). All mice were starved 5-6 hrs. SEM is based on three separate experiments. P<0.0035 for *Plp1*tgs, P>0.05 for jpTa compared to +/+ controls. Paired t-test.

Figure 2

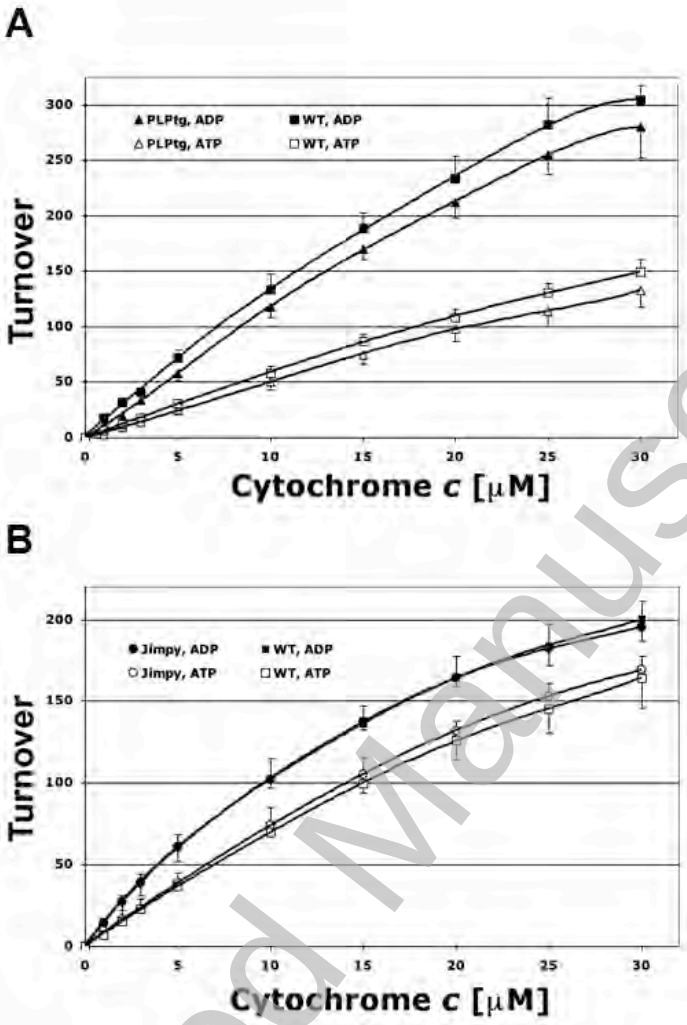

Figure 2. Cytochrome *c* oxidase (CcO) activities of mice starved for 5-6 hrs. CcO activity measurements used the polarographic method in the presence of 5mM ATP or ADP by increasing the amount of substrate cytochrome *c*. **A**. Comparison of CcO activities of wild-type (WT, squares, n=3) and *Plp1*tg mice (triangles, n=3) shows no significant difference in CcO activities in the presence of ATP (opens symbols) or ADP (closed symbols). **B**. CcO activities of jp mice (circles, n=5) is indistinguishable from wild-type animals (WT, squares, n=5) in the presence of ATP (opens symbols) or ADP (closed symbols). Turnover = consumed O_2 (μM/min/mg total protein).

ASN NEURO Immediate Publication. Published on 7 August 2009 as manuscript AN20090028

Figure 3

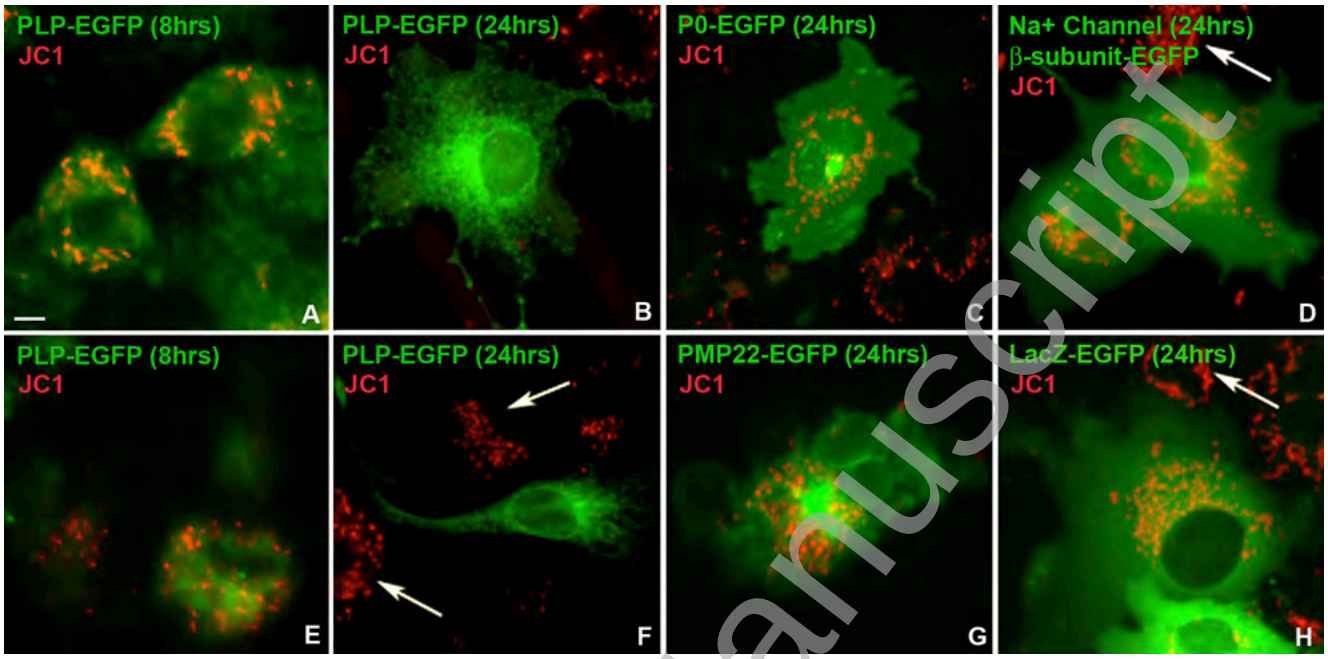

Figure 3. JC-1 staining of transiently transfected COS7 cells. **A, E**. Cells transfected with wild-type PLP fused to EGFP 8 hrs afterwards show abundant red stained mitochondria in cells expressing moderate levels of PLP. **B, F**. Twenty-four hrs after transfection with wild-type PLP-EGFP, most transfected cells express high levels of PLP and have abnormally low $\Delta\Psi_m$ indicated by loss of red stained mitochondria. Untransfected cells (arrows) show abundant red stained mitochondria indicative of normal $\Delta\Psi_m$ **(F)**. **C, G**. Cells transfected with myelin P0 protein **(C)** or PMP-22 **(G)** fused to EGFP show many red stained mitochondria, even in cells expressing high levels of EGFP. **D, H**. Cells transfected with the β-subunit of Na^+ channel fused to EGFP **(D)** or with LacZ-EGFP **(H)** show many red mitochondria. Arrows indicate non-transfected cells that have mostly red mitochondria. Magnification bar = 10 microns

ASN NEURO Immediate Publication. Published on 7 August 2009 as manuscript AN20090028

Figure 4

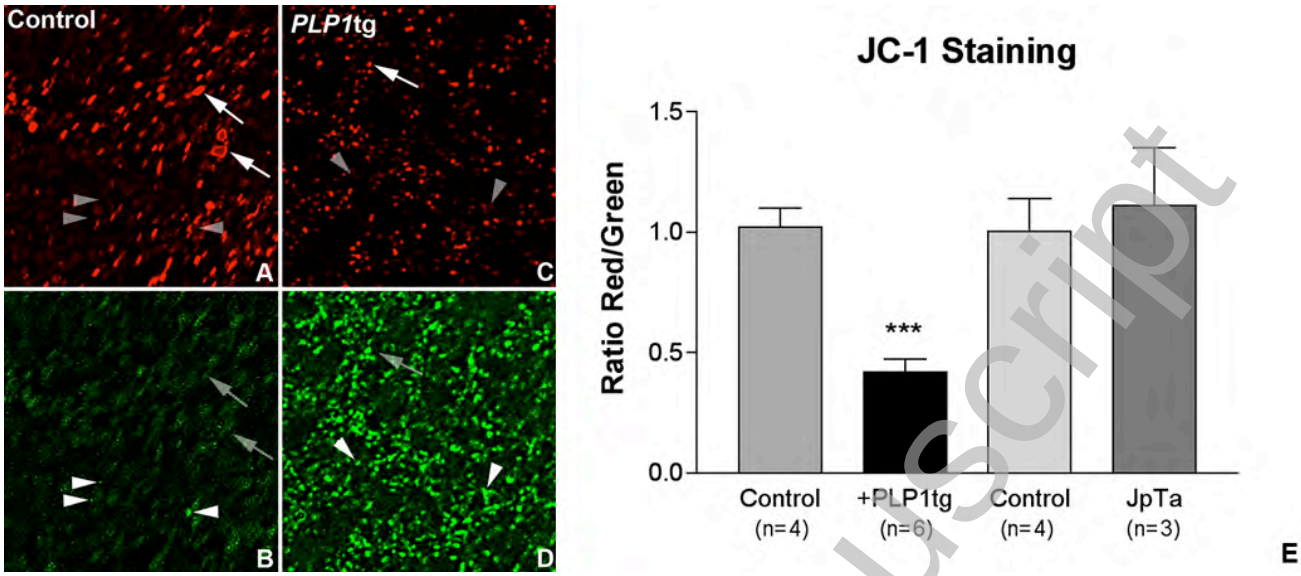

Figure 4. JC-1 staining of brain striata from strain matched controls **(A-B)** and *Plp1*tg **(C-D)** age-matched mice. One-hundred micron brain slices were stained with JC-1 dye within several minutes of harvesting brains. They were immediately imaged and images de-convolved at a later time. Red ellipsoids indicate relatively normal $\Delta\Psi_m$ and green ellipsoids represent a decrease in potential. Controls have few bright green mitochondria. Notice how "red stained" mitochondria in *Plp1*tgs occupies less area than in controls. Some mitochondria show only red fluorescence (arrows) and others only green fluorescence (arrowheads). **E**. Quantification of red to green ratio. n=number of animals. ***p=0.003, *PLP1*tg compared to wild-type PLP control, t-test.

FIgure 5

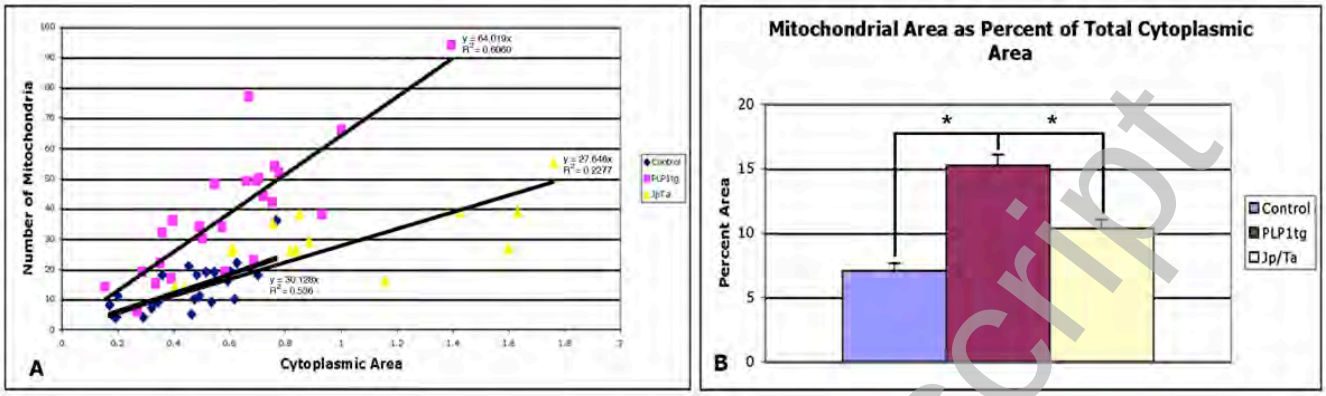

Figure 5. A. The number of mitochondria per mm^2 of Olg cytoplasm is increased more than two-fold in 35 day *Plp1*tg mice compared to both 35 day wild-type and jp mice. Each colored object represents the number of mitochondria contained within the total cytoplasmic surface area of one Olg. **B**. The sum of the mitochondrial area for each Olg was calculated and compared to its total cytoplasmic area. Significant difference of means for t-test: control and *Plp1*tg p<.0001; *Plp1*tg and jp/Ta p<.0001.

ASN NEURO Immediate Publication. Published on 7 August 2009 as manuscript AN20090028

Figure 6

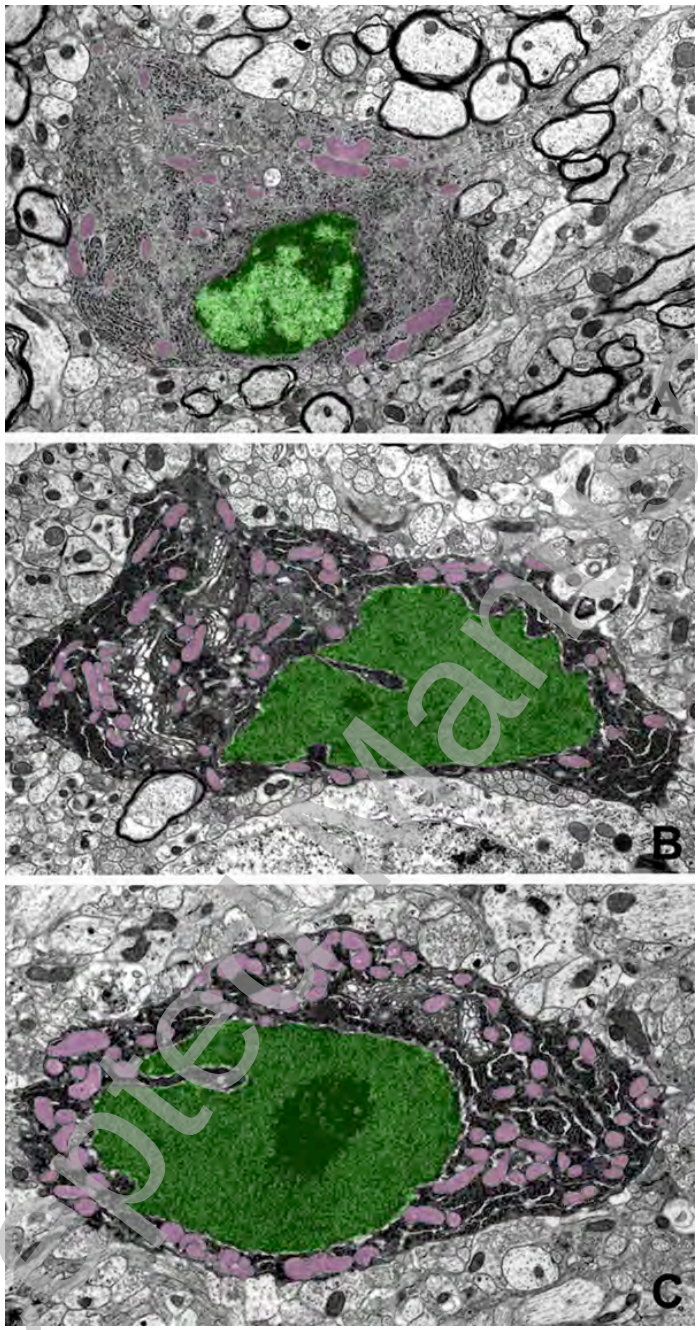

Figure 6. Electron micrographs of an Olg from a 35 day wild-type mouse **(A)** and Olgs from a 35 day *Plp1*tg mouse **(B-C)**. Nuclei are outlined in green and mitochondria in pink. The distribution of mitochondria and other organelles from the wild-type mouse is typical of normal Olgs. Although the cytoplasm and nuclei of *Plp1*tg Olgs are abnormally electron dense, their nuclei and plasma membranes are intact, suggesting they are still viable.

ASN NEURO Immediate Publication. Published on 7 August 2009 as manuscript AN20090028

Figure 7

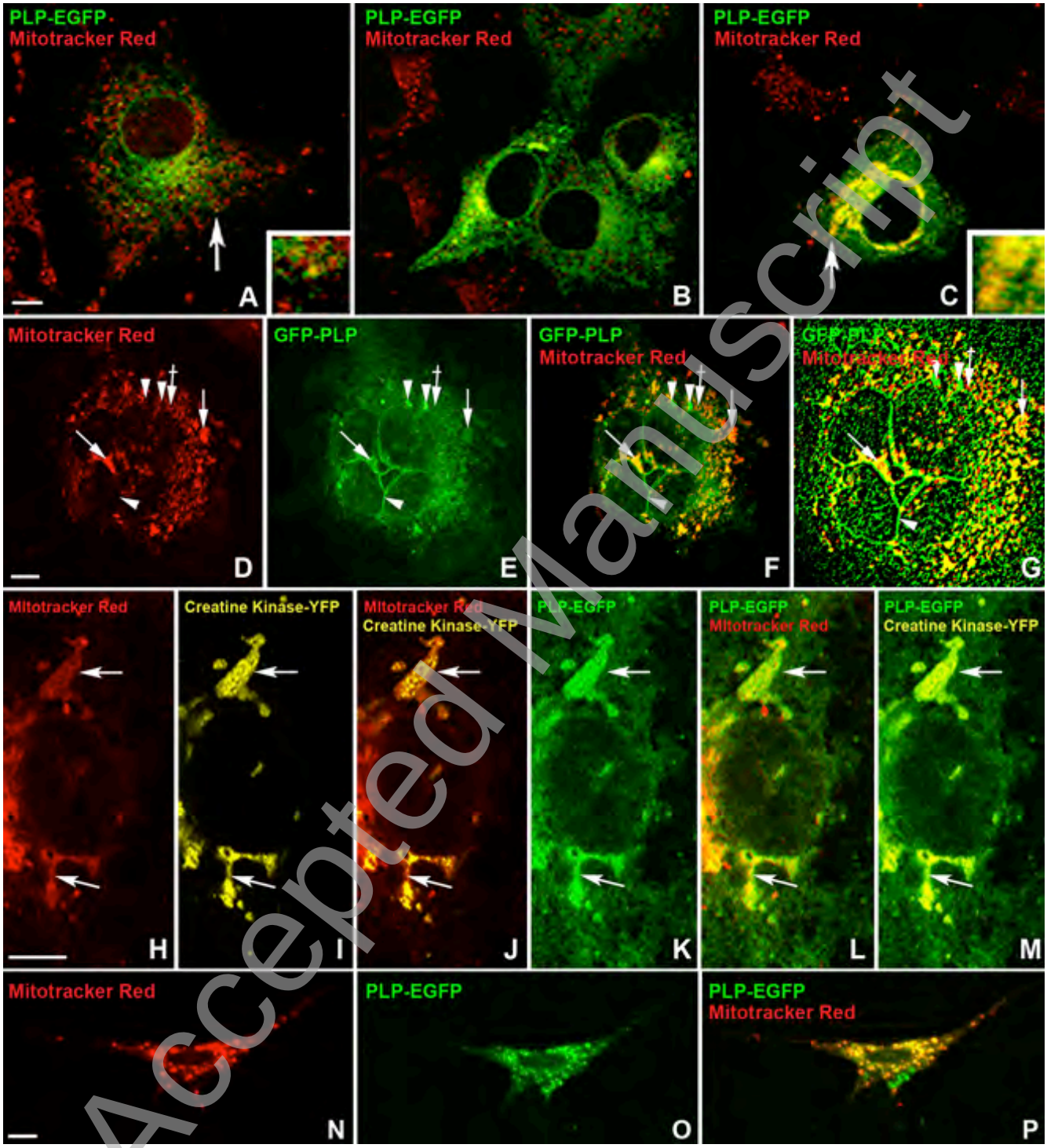

Figure 7. A-C. Confocal images of COS7 cells transiently transfected with a full-length PLP-EGFP construct and stained with Mitotracker Red. **A.** 12 hrs after transfection, most mitochondria in transfected cells stain red but some show co-localization with PLP (arrow and inset). Mitochondria in non-transfected cells are all red. **B-C**. By 36 hrs after transfection, co-localization is abundant (arrow and inset). **D-G.** COS7 cells transfected with GFP-full length PLP construct for 36 hrs and live stained for Mitotracker Red. Single channel confocal images **(D-E),** merged **(F),** and deconvolved **(G)** with Huygens Essential Software. **(D-G).** PLP-positive plasma membranes and cytoplasmic organelles (arrowheads) remain green in the merged and deconvolved images; some mitochondria remain red (crossed arrowhead) in the merged and deconvolved images. Co-localization of PLP and mitochondria (arrows) is abundant in merged confocal image. **G.** In the deconvolved image, green staining (PLP) surrounds yellow structures (PLP and mitochondria) that often surrounds a red portion of mitochondria. **H-M**. Confocal images of COS7 cells simultaneously transfected with creatine kinase-YFP and PLP-EGFP and stained with Mitotracker Red 580. **H-J**. Mitotracker Red and creatine kinase, visualized as canary yellow, co-localize as goldenrod **(J)**. A thin rim of red, presumably outer mitochondrial membrane, often surrounds inner mitochondrial membrane localized creatine kinase (arrows). **K-L**. Co-localization of PLP and Mitotracker Red produces yellow-orange staining. PLP (green) often surrounds the matrix localized creatine kinase staining (yellow) (arrows). **M**. Co-localization of PLP (green) and creatine kinase (canary yellow) produces a bright yellow staining. Green surrounds creatine kinase which has a worm-like configuration typical of mitochondrial cristae. **N-P**. Confocal pictures of oligodendrocyte cell line 158N transfected with PLP-EGFP and stained with Mitotracker Red. Single channel confocal images (**N-O)** and merged **(P).** Magnification bar = 10 microns

ASN NEURO Immediate Publication. Published on 7 August 2009 as manuscript AN20090028

Figure 8

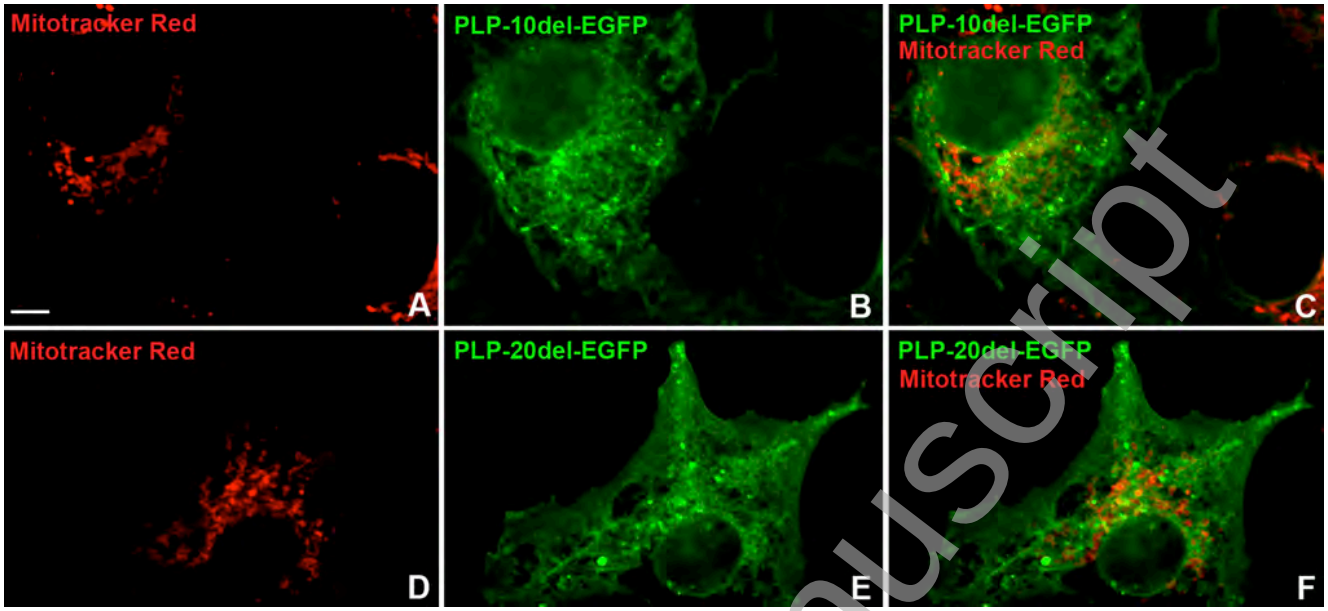

Figure 8. **A-F** Confocal pictures of COS7 cells transfected with the first ten **(A-C)** or first 20 **(D-F)** amino acids, exclusive of methionine, deleted from PLP and stained for Mitotracker Red 580. Most mitochondria are red and show no co-localization with PLP. However, faint yellow staining is present in some mitochondria. Truncated PLP is in vesicles that is transported into processes. Magnification bar = 10 microns

ASN NEURO Immediate Publication. Published on 7 August 2009 as manuscript AN20090028

Figure 9

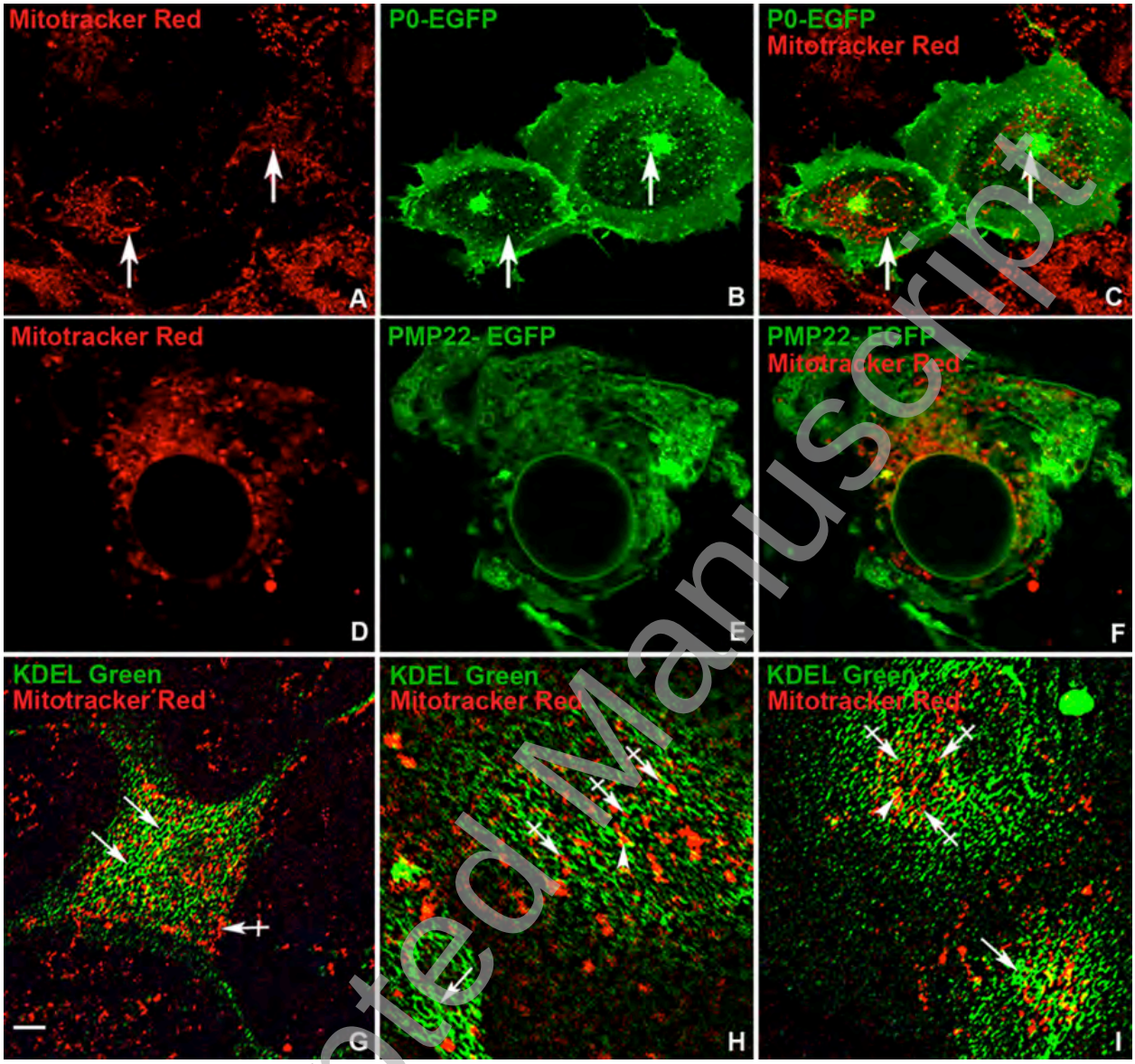

Figure 9. A-C. COS7 cells transiently transfected with P0-EGFP and stained with Mitotracker Red 580. **A**. Mitochondria are tubular or round structures spread throughout the cytoplasm but are often aggregated around the nucleus. **B**. P0 forms punctate dots throughout the cytoplasm, large and intensely fluorescent aggregates, and it also outlines the plasma membrane. **C**. In the merged image, mitochondria surrounding the nucleus are not co-labeled with P0 (left arrow), a single mitochondrion near the P0 aggregate (right arrow) is not co-labeled. **D-F**. COS7 cells transiently transfected with PMP22-EGFP and stained with Mitotracker Red 580. PMP22 and P0 do not co-localize with mitochondria in these confocal images except for occasional particles. **G-I**. Confocal, deconvolved images of COS7 cells stained for Mitotracker Red 580, fixed, and immunostained for KDEL using a FITC secondary. Reticulated pattern characteristic of ER (arrows) and tubular mitochondria (crossed arrows) often abut each other but do not co-localize. Close apposition of mitochondria with ER form occasional small dots (arrowheads) but do not show extensive overlap of PLP with mitochondria. Magnification bar = 10 micron

ASN NEURO Immediate Publication. Published on 7 August 2009 as manuscript AN20090028

Figure 10

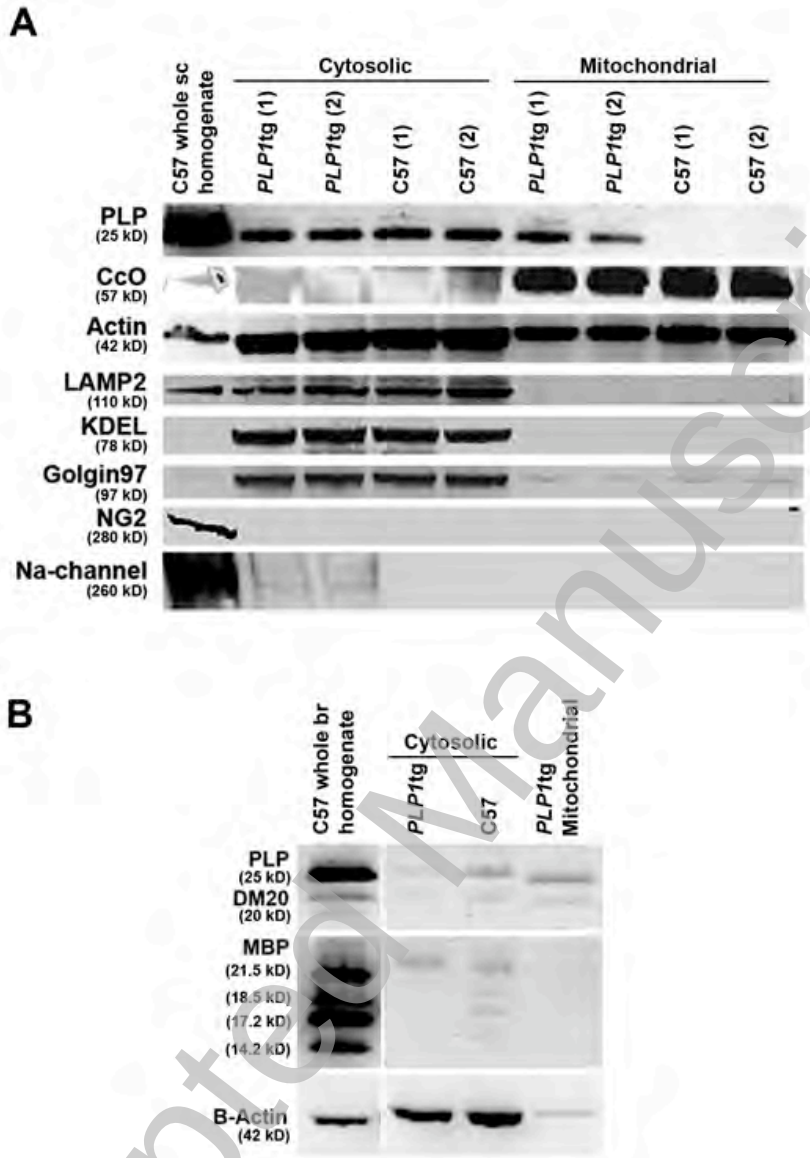

Figure 10. A. Immmunoblots of cytosolic and mitochondrial fractions of spinal cord of 60 day *PLP1*tg and wild-type C57 mice. Mitochondrial and cytosolic fractions were prepared using the Biovision Kit. The immunoblot was first probed with a PLP specific antibody, stripped, and subsequently reprobed for 5 other antibodies. The last 2 antibodies, because of their higher MW's, were run on a gradient gel using the same homogenate. **B.** Immunoblots of whole brain homogenates, cytosolic and mitochondrial fractions probed for PLP and MBP from 60 day C57 and *Plp1*tg mice. Antibody to carboxy terminus of PLP recognizes both PLP and DM20. PLP and DM20 MWs in mitochondrial fraction are slightly less than in whole brain or cytosolic fractions. Antibody to MBP recognizes all 4 MBP isoforms present in homogenate and cytosolic fractions in C57 mice but are absent in mitochondrial fractions. Actin in mitochondrial fraction is always less than in cytosol (see 10A above).

ASN NEURO Immediate Publication. Published on 7 August 2009 as manuscript AN20090028

Figure 11

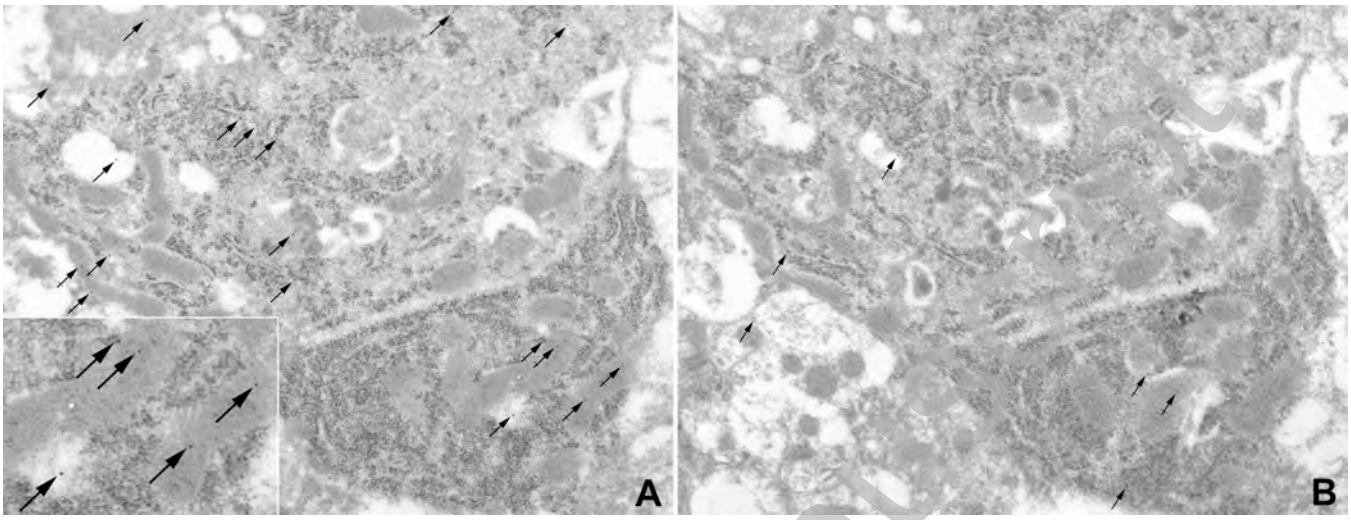

Figure 11. Electron microscopic immunogold sections from 35 day *Plp1*tg mice immunostained for PLP with 10μm gold particles using the post-embedding technique. **A-B.** Nearly adjacent sections show two Olgs with numerous gold particles overlying ribosomes and ER and mitochondria (arrows). Inset shows gold particles overlying mitochondria and a vacuole.

ASN NEURO Immediate Publication. Published on 7 August 2009 as manuscript AN20090028

Table 1

Location	% Increase *PLP1*tg over Control
Striatum DM	3.67
Striatum VL	8.13
Hippocampus	11.31
Corpus Callosum	18.97
Cortex	6.13

Table 1. Histochemical analysis of CcO in cerebrum from control (n=6) and *Plp1*tg mice (n=6) shows modest increased CcO density in *Plp1*tg (see Results).

ASN NEURO Immediate Publication. Published on 7 August 2009 as manuscript AN20090028

Table 2

Percent non-oligodendrocyte cytosolic structures w/ gold particles in mitochondria	Percent oligodendrocytes w/ gold particles in mitochondria
4	16.7

Table 2. Ultra-thin sections from 35 day *Plp1*tg corpus callosum and striatum were systematically scanned, all oligodendrocytes and surrounding neuropil were photographed, scanned, and photographically printed (see Figure 11). All immunogold particles overlying mitochondria were identified with a magnifying loupe and allocated to oligodendrocytes or to mitochondria in all other glia, axons, dendrites, and neuronal perikarya.